β-delayed particle decay of ^{9}C and the $A=9$, $T=1/2$ nuclear system: Experiment, data, and phenomenological analysis

E. Gete,[1,*] L. Buchmann,[2] R. E. Azuma,[3] D. Anthony,[4,†] N. Bateman,[2,3,4,‡] J. C. Chow,[3] J. M. D'Auria,[4] M. Dombsky,[2,4] U. Giesen,[2,5,§] C. Iliadis,[3,‖] K. P. Jackson,[2] J. D. King,[3] D. F. Measday,[1] and A. C. Morton[3]

[1]*Department of Physics and Astronomy, University of British Columbia, Vancouver, British Columbia, Canada V6T 1Z1*

[2]*TRIUMF, 4004 Wesbrook Mall, Vancouver, British Columbia, Canada V6T 2A3*

[3]*Department of Physics, University of Toronto, Toronto, Ontario, Canada M5S 1A7*

[4]*Department of Chemistry, Simon Fraser University, Vancouver, British Columbia, Canada V5A 1S6*

[5]*Department of Physics, University of Alberta, Edmonton, Alberta, Canada T6G 2J1*

(Received 3 June 1999; published 15 May 2000)

The β decay of ^{9}C ($T_{1/2}=126.5$ ms) has been studied in two experiments observing about 15×10^7 and 8×10^7 decays, respectively, at the TISOL facility at TRIUMF; different detector configurations were employed in the two experiments. In this first of two papers, the two experimental setups are described, as well as data analysis and a phenomenological approach to deducing branching ratios to and from states in ^{9}B. In the experiments single spectra, and double and triple coincidence spectra, were recorded. Several states in ^{9}B were observed; β-branching ratios to these states, and particle decay channels from these states, are reported. In particular, secondary decays into the ^{5}Li and ^{8}Be ground states were observed. With the inclusion of a considerable continuum and additional states, fair agreement with the reported ^{9}Li logft values is found with a phenomenological approach for deducing the branching ratios. To extend the discussion, in a second, forthcoming paper, a multichannel, multistate R-matrix analysis of these data will be described.

PACS number(s): 23.40.Hc, 27.20.+n

I. INTRODUCTION

A. General

In the $A=9$ isospin-doublet system, several states of the nucleus ^{9}B, which has only unbound states, have at present unknown spin-parity assignments or are not identified with mirror states in the nucleus ^{9}Be. In addition, the decay branches from states in ^{9}B are mostly not known. As far as β-decay studies are concerned, these uncertainties in nuclear properties are mainly due to the fact that the ^{9}C yield ($T_{1/2}=126.5$ ms) obtained in previous experiments was low and that, because of the three-body breakup, the particle spectra are kinematically broadened on top of already broad, unbound states in ^{9}B. In addition, several possible decay channels involving different kinematics further complicate the analysis. For these reasons, the β-decay scheme and logft values are poorly known for the different branches of the extremely proton rich nuclide ^{9}C ($Z/N=2$ being the highest proton-neutron ratio for a bound nuclide above ^{3}He). To illustrate this point, the level scheme associated with the decay of ^{9}C is shown in Fig. 1.

In two previous experiments [1,2] the explicit β-delayed proton emission from ^{9}C has been reported, with results from the high-energy portion of the proton spectrum. The proton spectrum of Ref. [2] exhibits several broad peaks some of which are consistent with states of ^{9}B known from other studies [3]. No β-delayed α emission of ^{9}C has been documented in the literature. In Ref. [4] it was reported that 10^4 ^{9}C ions had been implanted into a thick surface barrier detector and total decay energies had been measured for the low-lying states. The β-decay branching ratios for the ground state and the second and third excited states of ^{9}B were found to be $60\pm10\%, 17\pm6\%$, and $11\pm5\%$, respectively. A decay to a relatively narrow state with an excitation energy of about 12 MeV was also reported, in agreement with Refs. [1,2], but only a lower limit on the branching ratio was determined ($>1.8\%$). There has been an extensive study of the mirror ^{9}Li β-delayed particle decay [5]. Branching ratios to the mirror states of those observed by Ref. [4] differ for the second excited state in ^{9}B and are in marginal agreement for the other states with those of Ref. [5] (50, 30, 16% for the above states and 3.8% for the two $E_x\approx11$ MeV states). However, the results of Ref. [5] are based solely on the analysis of single neutron and α-spectra from which only a limited kinematic analysis can be obtained.

From a nuclear structure point of view, it has been argued that ^{9}Be is a Borromean system, i.e., a system held together only by the mediating neutron between the otherwise unbound pair of α particles [6–8]. States in ^{9}Be and ^{9}B can then be described in a way similar to covalent molecular states where, by analogy with the H_2^+ molecule, the neutron or proton, respectively, occupy with equal likelihood positions close to the α mass centers. Such a configuration, with the proton most of the time close to one of the α particles,

*Present address: London Regional Cancer Centre, London, Ontario, Canada.

†Present address: Michigan State University, East Lansing, MI.

‡Present address: Stringtown Road, Opoville, CA.

§Present address: University of Notre Dame, Notre Dame, IN.

‖Present address: University of North Carolina, Chapel Hill, NC.

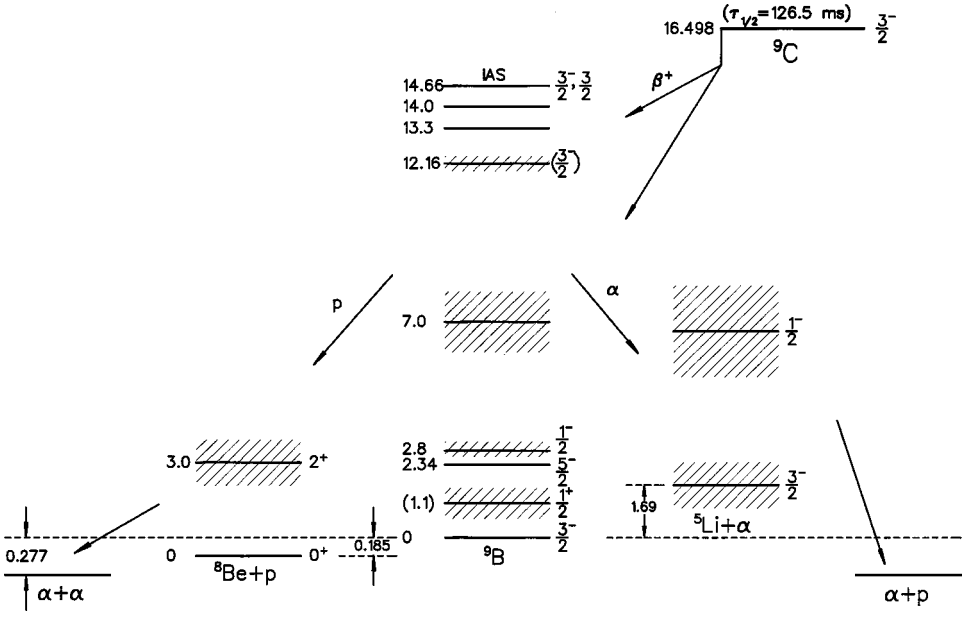

FIG. 1. Level diagram of ^{9}B [4], showing possible breakup modes of ^{9}B states through ^{8}Be and ^{5}Li . Spin-parity assignments of uncertain nature are in parentheses. A $J^\pi=5/2^+$ state at $E_x=2.7$ MeV in ^{9}B is not shown.

would correspond to a covalently bonded $^5\mathrm{Li}+\alpha$ ''molecule.''

There has been considerable controversy about the energy and width of the first excited state of ^{9}B ($E_x \approx 1-2$ MeV, $J^\pi=1/2^+$) [3,9–12],[13][1] with Refs. [9,10] claiming its observation in transfer reactions. A recent experiment [11], however, did not find any evidence to support this claim, while in Ref. [12], employing transfer reactions and three-particle coincidences, the decay of this state via $^8\mathrm{Be}+p$ has been indicated. This state should not be strongly populated in the β^+ decay of ^{9}C as the decay would be first forbidden. However, because of the high Q value, a population in the range of 1% is possible. Reference [5] places an upper limit of 2% in the β decay of ^{9}Li to the first excited state in ^{9}Be. Most of the theoretical and experimental discussion centers around the possible energy of the first excited state, and it normally seems to be assumed that this state decays solely via the ^{8}Be ground state in a two-step process.

Another reason for investigating the $A=9$ system is that, in the entropy rich bubble between a cooling neutron star and the shock wave from the preceding supernova core collapse, the rapid buildup of heavy isotopes initiated by the $^4\mathrm{He}(\alpha n,\gamma)^9\mathrm{Be}$ reaction leads to the formation of seed elements around mass $A=80$ for the r process [14]. To determine the stellar reaction rate of this reaction ($T\approx 3$ GK), the properties of the low-lying, unbound states in ^{9}Be are very important, i.e., the properties of the lowest lying $J^\pi=1/2^+, 5/2^-, 1/2^-$, and other states. The derivation of this reaction rate will be discussed in a forthcoming paper [15].

B. Objectives and layout of the paper

The major experimental objectives of the present work are the identification of the excited states of ^{9}B along with the determination of their properties (e.g., energies, widths, spins and parities, and particle decay modes), and the measurement of the β-decay branching ratios of ^{9}C to these states in ^{9}B.

In Ref. [4] it was pointed out, correctly, that to achieve these objectives the acquisition of single-particle spectra is not sufficient, as kinematic broadening severely distorts the spectra and leads to ambiguous interpretations. As the ^{9}C β decay occurs at rest in the laboratory, for each state populated in ^{9}B the sum of the energies of the two α particles and the proton from the decay of the ^{9}B daughter nucleus is independent of the successive decay mode when the full solid angle is covered (ignoring the small ^{9}B recoil energy from the β decay, which depends on the β-ν angular correlation). A summed energy measurement was indeed achieved in Ref. [4], but at the price of losing all kinematic information in the sum spectrum. Such kinematic information is crucial for any theoretical understanding of the spectra, because the spectra which are eventually obtained cannot be properly interpreted without knowledge of the separate decay channels. For example, it is easy to see that the penetrabilities for decay channels leading to states in ^{8}Be and ^{5}Li, used in such calculations, are quite different from one another.

To accomplish the objectives of the present paper, two experiments with different detector geometries were performed at the TISOL facility at TRIUMF, which provided previously unavailable yields of ^{9}C, and data were taken and recorded in an event-by-event mode to allow full kinematic reconstruction and analysis. This also allowed the simultaneous collection of singles, and double and triple coincidence spectra. The experimental setups for these two experiments (henceforth identified as expt. 1 and expt. 2) are described in Sec. II. After a short description of the TISOL facility and the production of radioactive beams (Sec. II A), a description of the detection systems (Sec. II B), electronics and data acquisition systems (Sec. II C) is presented . Energy calibrations are discussed in Sec. II D. The model adopted for describing broad states is discussed in Sec. III A, and

[1]See references therein for theoretical discussion.

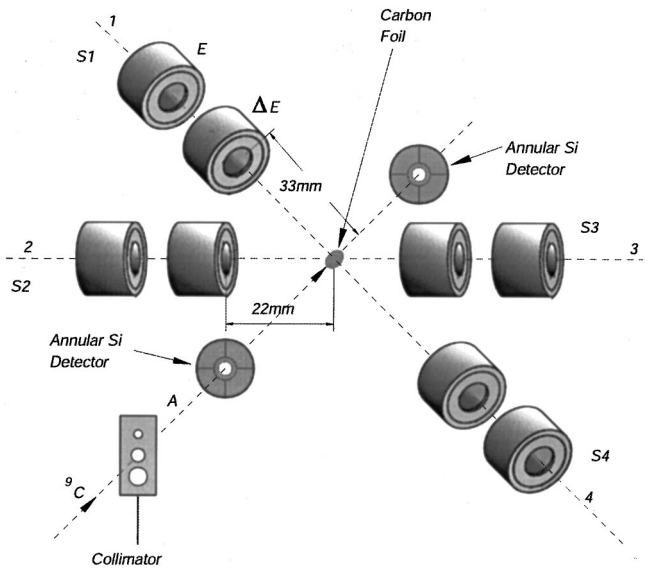

FIG. 2. Detector configuration and geometry for expt. 1. The beam line and detectors S2 and S3 define a horizontal plane for detecting decay products, with the S2-S3 detector pair at 90° to the beam line. The beam line and detectors S1 and S4 form a second plane rotated at 45° about the beam line with S1 above the horizontal. In this second plane the S1-S4 pair is rotated clockwise at 45° with respect to the S2-S3 pair.

angular correlations are discussed in Sec. III B. Monte Carlo simulations were performed as described in Sec. III C.

It will be seen below that there are two dominant kinematic modes of breakup of the states of ^{9}B, i.e., decay through the ground states of either ^{8}Be or ^{5}Li and the first excited state of ^{8}Be at 3 MeV. It is shown that the geometry of expt. 1 can be exploited to select kinematically only the breakup through the ground state of ^{8}Be, while that of expt. 2 can be used to select preferentially breakups through the ground state of ^{5}Li and the ^{8}Be(3 MeV) state. The data analyses for these two experiments are discussed in Secs. IV A and IV B, respectively, with the results of expt. 1 shown in Fig. 7, and those of expt. 2 in Fig. 8. The results presented in these two figures account for more than 40% of the β decays of ^{9}C. In addition to these modes of decay, it was known from previous work that β decay to the ground state of ^{9}B could account for about 50% of the total β decays. This is corroborated in the data described in Sec. IV C and shown in Fig. 12. Angular correlation results for the $E_x = 12.2$ MeV state are presented in Sec. IV D. Weak branches to the first excited and high-lying states of ^{9}B are discussed in Sec. IV E. These three sets of results, Figs. 7, 8, and 12, are then combined in Sec. V to give the final β-decay branching ratios as well as the experimental energies, widths, and particle-decay branching ratios for the states of ^{9}B. Conclusions are presented in Sec. VI.

II. THE EXPERIMENTAL SETUP

In this section the ^{9}C beam production and the setup and energy calibrations of the two experiments are described. The two experiments used the same production method for the ^{9}C beam but differed in their detector configurations and electronics.

A. ^{9}C production at TISOL

A beam of ^{9}C ($\leqslant 10^4$ s^{-1}) was extracted from the TRIUMF isotope separator TISOL, which employed a 13 g/cm^2 zeolite production target. The TISOL ECR ion source [17,18] was operated with a 12 kV extraction voltage. After extraction and mass separation, the beam was transported to the collection station and implanted into a thin carbon foil. During expt. 1 the ion beam was deflected off the collector foil periodically for a small fraction of the run time in order to test for the presence of longer-lived contaminant beams. No protons or α particles from the decays of long-lived nuclides were identified. A liquid nitrogen trap and a collimator were mounted upstream close to the detector station to improve the vacuum and minimize carbon deposits on the beam collector foil. A Faraday cup downstream from the collector foil assisted with the focusing of the ion beam. With the 12 keV mass $A=25$ $(^9C^{16}O)^+$ beam[2] from the TISOL isotope separator, the 10 μg/cm^2 C foils did not show any sign of deterioration in the course of the experiment as there was no significant stable ion beam at this mass position (<1 nA). However, strong yields of the short-lived radioactive isotopes ^{11}C [$T_{1/2}=20.4$ min, $(^{11}C^{14}N)^+$] and ^{13}N[$T_{1/2}=10.0$ min, $(^{12}C^{13}N)^+$] were observed at this mass position. These two isotopes caused considerable β background in the low-energy regions of detection.

B. Detection systems

The study of the β-delayed particle decay of ^{9}C requires a detection system that is capable of measuring protons and α particles over the range from 100 keV to 14 MeV with good energy resolution and coincidence efficiency. Therefore, silicon detectors were chosen for these experiments.

In order to provide charged-particle identification, ΔE-E telescopes consisting of pairs of thin and thick surface-barrier detectors were used. For particles that do not have sufficient energy to pass entirely through the front detector, particle identification was not always possible. Even though most of the β particles fully traversed both detectors of the telescopes, energy cuts on the two-dimensional plots of ΔE vs E were extremely useful in significantly reducing β events since these occurred in the lower-energy region of the plots away from the protons and α events. In addition to the silicon detector telescopes, segmented annular silicon detectors were used in expt. 1, while double-sided silicon strip detectors (SSDs) were used in expt. 2. Also in expt. 2, a plastic scintillator of sufficient thickness to stop the highest energy β particles was used.

In the first experiment a multidetector setup [16] was built around the thin collector foil in which the ion beams were stopped. The setup consisted of a movable target ladder holding several carbon foils and an α-calibration source, and

[2]No ^{9}C was observed at the $A=9$ mass position.

four detector stations with two back-to-back pairs as well as a pair of annular detectors positioned on the beam axis also in back-to-back geometry.[3]

Protons and high-energy α particles were detected in the ΔE-E telescopes. The ΔE (front) detectors were either 10 or 30 μm thick, while the E counters were 1500 and 2000 μm thick to exceed the full range of the protons. The annular detectors were 300 μm thick. The setup for expt. 1 is shown in Fig. 2.

The electronics and data acquisition system (see Sec. II C) permitted data to be extracted for many different combinations of detectors in coincidence simultaneously. However, the back-to-back coincidence combination of two telescopes was found to be of major importance in the subsequent analysis, since this coincidence combination was extremely effective in selecting events associated with the breakup of ^{9}B states through the ground state of ^{8}Be. Hence, the two coincident pairs S1-S4 and S2-S3 were chosen to provide the data for these analyses. This is discussed in detail in Sec. IV A.

The main features of the second experiment were the use of silicon strip detectors and the additional detection of β particles with a thick plastic scintillator. A pair of ΔE-E telescopes as described above, as well as two double-sided silicon strip detectors[4] (300 μm thickness) were used for detection of protons and α particles. The SSDs are made by etching several individual electrodes onto the surface of a rectangular silicon wafer both on its front and back. Dividing the electrodes into several pieces results in a corresponding geometric division of the charge-collecting electric field. The position of interaction is then localized as having occurred in the detector element where the electrode strips cross. At room temperature the strip detectors posed some problems because of high leakage currents, especially when some stable ion beam from the separator was present. Therefore, a cooling system was designed to keep the SSDs at about 4°C.

Each SSD was placed back-to-back with respect to a ΔE-E telescope. The collector foil was located near the midpoint between the two detectors and oriented perpendicular to the beam direction. The β detector was placed directly along the beam direction. A schematic of the experimental setup for expt. 2 is given in Fig. 3. The detectors are referred to in the text with the labels given on this figure. Triple coincidences were selected to provide most of the information for this run. This is discussed in detail below in Sec. IV B where it is shown that this setup preferentially selects

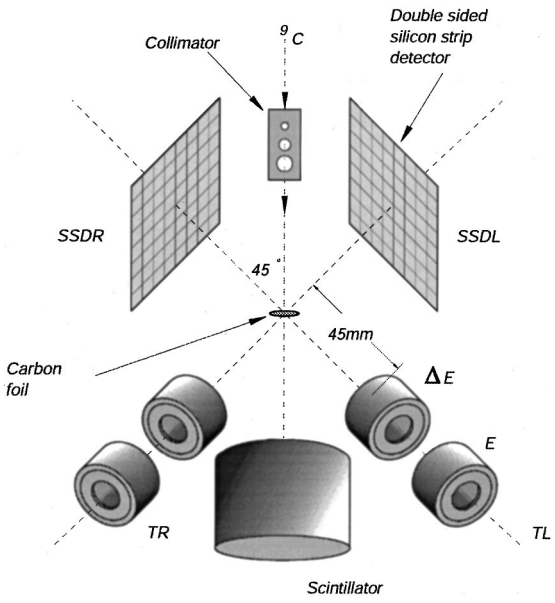

FIG. 3. Detector configuration and geometry for expt. 2. SSD labels double-sided silicon strip detectors (see text) and T labels ΔE-E telescopes. The beam line and the center lines of the detectors are all in the horizontal plane.

decays through the ground state of ^{5}Li and the ^{8}Be (3 MeV) state.

C. Electronics and data acquisition systems

In expt. 1 each detector was connected to the data acquisition system using an Ortec 142B preamplifier, located outside the vacuum chamber. The detectors were electrically isolated from the support structure and from the vacuum feed-through plate. A precision pulser signal was fed to the test input of each preamplifier. The energy signal from each preamplifier was sent to a spectroscopy amplifier. The output signals from these amplifiers were then sent to spectroscopic ADCs where their energy-dependent amplitudes were digitized and recorded. The timing signals obtained from the preamplifiers were sent through timing filter amplifiers and constant fraction discriminators (CFDs). The CFD output of any of the front detectors and, with a high threshold, the back detectors could trigger the data acquisition system to read out all detectors. The CFD output signals were also sent to TDCs. In the data analysis, appropriate cuts were placed on the time spectra of coincidence events between front detectors.

The electronics for the telescope detectors in expt. 2 were similar to those used during expt. 1. The signal from the β detector was included in the trigger logic. The SSDs were not included in the trigger logic due to the high β-induced count rate observed by these detectors. The SSD signals were fed to charge sensitive preamplifiers and then to shaping amplifiers.[5] These shaping amplifiers use leading-edge discriminators to generate timing pulses. Both timing and am-

[3]''Back-to-back geometry'' or similar expressions are used to describe the configuration of a pair of detectors which are located on a straight line facing each other with the ^{9}C collection target located near the midpoint of the line. This geometry is kinematically favored, because in a two body breakup the particles will emerge back-to-back leading to signals in both detectors. If the secondary breakup has little energy compared to the primary, the primary and at least one of the two secondary particles will likely decay in a way that they are detected in a back-to-back geometry.

[4]By Micron Inc., Marlborough Road, Royal Buildings, Churchill Industrial Estate, Lancing, Sussex, U.K., BN15 8UN.

[5]Acquired from Rutherford Appleton Laboratory.

plitude information were recorded for each triggered event.

The data acquisition system used in both experiments consisted of a single-crate CAMAC acquisition system, a PDP-11 CPU housed in the CAMAC crate (Starburst), and a VAX workstation. The VAX computer was used for online monitoring, data storage and downloading of user-defined programs to the Starburst unit. For each trigger event, the energy and timing signals from each detector were digitized and recorded on an 8 mm VCR tape. An event bit pattern, which was used to identify the detector signal that caused the trigger, was also recorded. Online monitoring was performed using the TRIUMF-developed analysis program NOVA, which allows the user to provide the definition of various spectra as well as conditions or cuts to be imposed on the data to select events for inclusion into specific histograms. This analysis software was also used later for the offline analysis. Events selected as valid were then written out in ASCII format and made subject to the more thorough kinematical analysis described below (Sec. IV).

D. Energy calibrations

Accurate determination of the energies of the particles being measured is a very important aspect of these experiments as the state energy of ^{9}B, as well as its breakup mode, is determined from the energy and the direction measurements of the decay particles. Because of different stopping powers and pulse height defects, separate energy calibrations for α particles and protons were performed.

Proton and α peaks from the β-delayed particle decay of ^{17}Ne [19] as well as the α peaks from the β-delayed decay of ^{18}N [20] were used for calibrations in both experimental runs. In addition, α-particle energy calibrations were performed with ^{241}Am and ^{148}Gd sources which emit 5485.7 and 3182.8 keV α particles, respectively [16]. For the telescopes, the α-particle calibration for the front detectors and the annular detectors was performed using the ^{18}N peaks and the peaks from ^{241}Am and ^{148}Gd.

In contrast to the ^{17}Ne spectrum, the ^{18}N spectrum has only two major α peaks at 1081.0 and 1409.0 keV [20]. These are very suitable α calibration peaks for the present experiment as most of the α particles from the decay of ^{9}C are in this energy range. These α peaks have very small natural linewidths, and are slightly broadened kinematically by the β-ν recoil, depending on the β-ν angular correlation.

III. METHODS USED IN THE ANALYSIS

A. Fitting procedures and decay through broad states

In this first of two papers on the decay of ^{9}C, a simplified method of fitting the experimental spectra has been used. Although this method is based on the formalism given in Ref. [21], for computational reasons, as further discussed in Sec. V, the following simplifications have been introduced: the multichannel aspect of the problem is ignored, i.e., only diagonal elements of the state matrix **A** are included; also, only one state per angular momentum J^π was considered, resulting in a sum over noninterfering, single-state terms. Boundary conditions were set equal to the shift function for the single-state energies. For the energy scale, the ground state of ^{9}B was set to zero, labeling energies relative to it by E. Since the decay of states in ^{9}B, however, proceeds through intermediate states with an energy $E_{\rm int}$, which decay to the $2\alpha+p$ system, an energy E' relative to the $2\alpha+p$ mass was introduced. Then, $E_{\rm int}+Q=E'$, with $Q=0.277$ MeV, the breakup energy of ^{9}B. For the simple case of a ^{8}Be ground state transition, therefore, $E_{\rm int}=-0.185$ MeV and $E'=0.092$ MeV. Then, in agreement with Ref. [5] for one state,

$$W(E,E')=Af_\beta(E)\frac{P_9(E-E_{\rm int})\gamma^2 w(E')}{[E-E_R-\Delta_9(E)]^2+[\Gamma(E)]^2/4}, \tag{1}$$

where $W(E,E')$ is the energy distribution of particles in the $A=9$ system and $w(E')$ is that in the intermediate system; A is an arbitrary feeding factor scaling to the spectrum and γ is the reduced width amplitude. P_9 labels the appropriate penetrabilities in the $A=9$ system and is channel dependent. The formal widths, $\Gamma(E)$, and the relative shift function, $\Delta_9(E)$, in Eq. (1) are given by the one-level R-matrix expressions

$$\Gamma(E)=2\gamma^2 P_9(E-E_{\rm int}) \tag{2}$$

$$\Delta_9(E)=-\gamma^2[S_9(E-E_{\rm int})-S_9(E_R-E_{\rm int})], \tag{3}$$

with E_R being the resonance energy. The (absolute) shift functions $S_9(E)$ and the penetration factors $P_9(E)$ are calculated from the regular and irregular Coulomb functions (the interaction radii used here are $a=1.4(A_1^{1/3}+A_2^{1/3})$ and are strong functions of the breakup energies [22]). $w(E')$ represents the breakup through the intermediate state as

$$w(E')=\frac{P_i(E')\gamma'^2}{[E'-E_{R'}-\Delta_i(E')]^2+[\Gamma'(E')]^2/4}, \tag{4}$$

with P_i being the penetrability from the intermediate state, again channel dependent. For the decay of the narrow ^{8}Be ground state, $w(E')$ reduces to an energy independent number; then, $W(E,E')\rightarrow W(E)$.

The situation for a decay through broad states [e.g., ^{5}Li(g.s.)] is not so straightforward. As seen above, the calculations involve the product of the penetrabilities for formation and decay of the intermediate state. For decay through broad states, Eq. (1) above is used, but the product of the penetrabilities is replaced by the mean value calculated by weighting the product with the shape function of the intermediate state, following Refs. [5,21–23]. For a given excitation energy E in ^{9}B and resonance energy $E_{R'}$ for the broad intermediate state, this mean value is given by

$$\langle P_9(E-E_{\rm int})P_i(E')\rangle=\frac{\int_0^{E+Q}P_9(E-E_{\rm int})w(E')dE'}{\int_0^{\infty}w(E')dE'}. \tag{5}$$

Note that the integral in the numerator also extends in principle to ∞. Inserting Eq. (4) into Eq. (1) and employing the mean value of the penetrabilities according to Eq. (5) then leads to the desired distribution $W(E)$. Such distributions were later summed for each state and channel.

For the branching ratio determination via Monte Carlo simulations, simplified distributions were used (see Sec. VA). For ease of calculation in both the Monte Carlo simulations and the least squares fitting of peaks for decays through ^{5}Li(g.s.), the mean product of penetrabilities was calculated beforehand for all the experimental excitation energies in ^{9}B from 2.0 to 14.0 MeV.

B. Angular correlations

In triple coincidences of particles in sequential decays, the angular correlations between the particles need to be taken into account. A thorough discussion of such angular correlations is found in Ref. [24]. Even for those cases where the spins of the states are known, the correlations are complicated by the fact that, in most cases, several channel spins, and hence several orbital angular momenta, are allowed which mix coherently in the correlations [15]. In the Monte Carlo calculations presented here for both the detection efficiencies and the determination of spins, only the lowest of the allowed l values was assumed to play a role.

The angular correlation is then given by [Eq. (15.6) of Ref. [24]:

$$W_{\mathcal{L}_1\mathcal{L}_2}(\theta)=(4\pi)^2(-1)^{a+c-2b}(2b+1)\sum_{k=2i}(-1)^{-L_1-L_2}\times C_{k0}(\mathcal{L}_1\mathcal{L}_1)C^*_{k0}(\mathcal{L}_2\mathcal{L}_2)W(bbL_1L_1;ka)\times W(bbL_2L_2;kc)P_k(\cos\theta). \quad (6)$$

In Eq. (6), θ is the angle between the first and the second breakup. a, b, and c are the spins of the states of the three nuclei involved in the cascade transition. L_1 and L_2 are the total angular momenta of the emitted particles. $\vec{L}_i=\vec{l}_i+\vec{s}_i$ where $\vec{l}_i$ and $\vec{s}_i$ are the orbital angular momenta and the intrinsic spins of the particles, respectively. $\mathcal{L}$ denotes the set of angular momenta L and l. Furthermore, $W(bbL_1L_1;ka)$ are the Racah coefficients. The coefficients $C_{k0}(\mathcal{L},\mathcal{L})$ are given by

$$C_{k0}(\mathcal{L},\mathcal{L})=\frac{2L+1}{4\pi}(-1)^l(l0,l0|k0) \quad (7)$$

for α particles, and

$$C_{k0}(\mathcal{L},\mathcal{L})=\frac{2L+1}{4\pi}(-1)^{L-1/2+k}\left(L\frac{1}{2},L-\frac{1}{2}\middle|k0\right) \quad (8)$$

for protons. $P_k(\cos\theta)$ are the usual Legendre polynomials of $\cos\theta$. The selection rule for the sum over k requires that k be even and the maximum of k is given by

$$k_{\max}=\min(2L_1,2l_1,2L_2,2l_2,2b). \quad (9)$$

TABLE I. Angular correlations in terms of the Legendre polynomials $P_2(\cos\theta)$ and $P_4(\cos\theta)$ for the breakup of ^{9}B states into an intermediate (daughter) nucleus; only the lowest allowed orbital angular momenta were included in the computations.

J^π of ^{9}B state	Intermediate nucleus	Angular correlation
$\frac{1}{2}^-$	^{5}Li($\frac{3}{2}^-$)	$1+P_2$
$\frac{3}{2}^-$	^{5}Li($\frac{3}{2}^-$)	1
$\frac{5}{2}^-$	^{5}Li($\frac{3}{2}^-$)	$1-0.7141P_2$
$\frac{1}{2}^+$	^{5}Li($\frac{3}{2}^-$)	$1+P_2$
$\frac{1}{2}^-$	^{8}Be(2^+)	$1+P_2$
$\frac{3}{2}^-$	^{8}Be(2^+)	1
$\frac{5}{2}^-$	^{8}Be(2^+)	1,$1-0.7141P_2$ [a]
$\frac{1}{2}^+$	^{8}Be(2^+)	$1+P_2$, $1+1.1427P_2+0.8568P_4$ [a]

[a]For the two possible couplings of the proton to the angular momentum.

Because $J^\pi=0^+$ for the ^{8}Be ground state, all angular correlations through this state will be isotropic. Decays through the ^{5}Li ground state ($3/2^-$) and the ^{8}Be(2^+) state can show an angular distribution of the pattern:

$$W(\theta)=a_1+a_2P_2(\cos\theta)+a_4P_4(\cos\theta), \quad (10)$$

with the angular correlation coefficients $a_{1,2,4}$, respectively, derived from Eq. (6). Table I lists the angular correlation for the different levels in ^{9}B decaying through various channels. Only Legendre polynomials to second order are found for the lowest angular momenta considered here, except for the ^{8}Be(3 MeV)$+p$ case and $J^\pi=1/2^+$.

C. Monte Carlo simulations

Because the initial beam ions are stopped completely in the catcher foil, the laboratory and center-of-mass system are identical in the β decay of ^{9}C. After the β decay, the ^{9}B nucleus has a small ($\beta+\nu$) recoil momentum which has been ignored in the kinematics calculations. The breakup of the recoiling fragment of the ^{9}B breakup is viewed in its own moving reference frame. The kinematic variables are then transformed into the laboratory frame with the application of momentum and energy conservation. This leads to

$$\frac{m_2}{m_3(m_2+m_3)}Q_2-\frac{m_1}{(m_2+m_3)^2}E_1-\frac{1}{m_3}E_3=\frac{2}{m_2+m_3}\sqrt{\frac{m_1}{m_3}E_1E_3}\cos\phi \quad (11)$$

with the index 1 for the stable fragment of the first breakup, the index 3 for one of the particles of the second breakup, and index 2 for the other. Q_2 is the total energy of the second breakup and ϕ is the laboratory angle between particles 1 and 3.

In the case where the breakup of ^{9}B leaves the recoiling fragment in a narrow state, Q_2 is well defined. Then, for a given excitation energy in ^{9}B and a given value of ϕ, the energies of particles 1 and 3 are uniquely defined and would be represented by a single point in a two-dimensional plot of $E1$ vs $E3$. On the other hand, if the second breakup is through a broad state, Q_2 can have a range of values determined by the width of the state, and the energies of the breakup particles would lie on an extended locus in the $E1$-$E3$ plot. In an experiment, the distributions of particles along possible loci are modified by the shape functions of the secondary states (Sec. III A) as well as by the finite solid angles of the detectors and the finite size of the source.

As noted above, in addition to the possibility of decays through broad secondary states, the experiment is further complicated by the fact that β decay does not leave ^{9}B only in sharp states but rather with a combination of narrow and broad states along with a continuum of excitation energies in ^{9}B. The interpretation and analysis of coincidence spectra hence becomes extremely complex. One possible way to surmount these difficulties is to perform extensive Monte Carlo calculations which simulate the decay of ^{9}B through all the possible channels for the appropriate choice of excited states in ^{9}B.

A computer program was therefore written to simulate the breakup of ^{9}B via each of the several decay channels available, with the experimental geometry for the two experiments incorporated in the simulations. In a typical simulation, several million events were calculated. A Gaussian source density with circular symmetry was sampled. Particles from the first ^{9}B breakup were assumed to be emitted isotropically. Where necessary, both angular distributions and widths of states were sampled for the subsequent breakup. For the widths, the probabilities were sampled according to the distributions given in Sec. III A. The angular distribution probabilities are given in Sec. III B and were also included in the simulations. After all events were calculated, the geometric constraints of the detectors and electronic detection thresholds were applied to make the final selection of events for each decay channel. The Monte Carlo efficiencies and detector spectra were determined from these selected events. For the efficiency curves used below (Fig. 6 and Fig. 9), 2 million events were calculated for each point on the curves. For the breakup chain via ^{8}Be(g.s.) in expt. 1, neither angular correlations nor state shape functions were required and the process was straightforward. However, for expt. 2 where the breakup chain is mainly via ^{5}Li($3/2^-$), the situation is more complicated. This is discussed in detail in Sec. IV B.

Different kinds of simulations were done mainly for three interrelated reasons. First, the coincidence detection efficiency is a function of the excitation energy in ^{9}B, the particle breakup mode, the energy available in the decays and the experimental geometry. Monte Carlo simulation was the only practicable option available to determine these efficiencies. Second, Monte Carlo simulations of the various breakup modes including the calculated efficiencies had to be used to determine the β-decay branching ratios to states in ^{9}B, and the particle decay branches of these states by adjusting the input parameters of the Monte Carlo simulations until they reproduced the experimental spectra. Finally, simulations were used to determine the angular correlations of the breakup modes of each ^{9}B state by making comparisons between the experimental and simulated singles spectra and the coincidence spectra. These angular correlation data were useful for limiting spins and parities of the ^{9}B states [16] (see Sec. IV D).

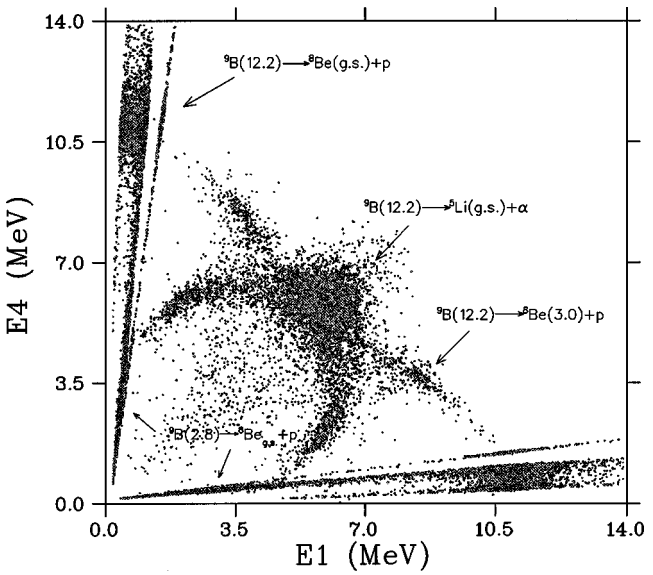

FIG. 4. Scatter diagram of simulated double coincidence spectra for detector telescopes S1 and S4, the back-to-back detector pair with the larger distance from the center of the ^{9}C collection foil in the expt. 1 geometry. The simulated events include (i) ^{9}B(12.2) $\rightarrow$ ^{8}Be(g.s.)+p, (ii) ^{9}B(12.2)$\rightarrow$ ^{5}Li+α, (iii) ^{9}B(12.2)$\rightarrow$ ^{8}Be(2^+) +p, and (iv) ^{9}B(2.8)$\rightarrow$ ^{8}Be+p. The number of simulated events is (i) 2×10^6, (ii) 4×10^6, (iii) 4×10^6, and (iv) 4×10^6.

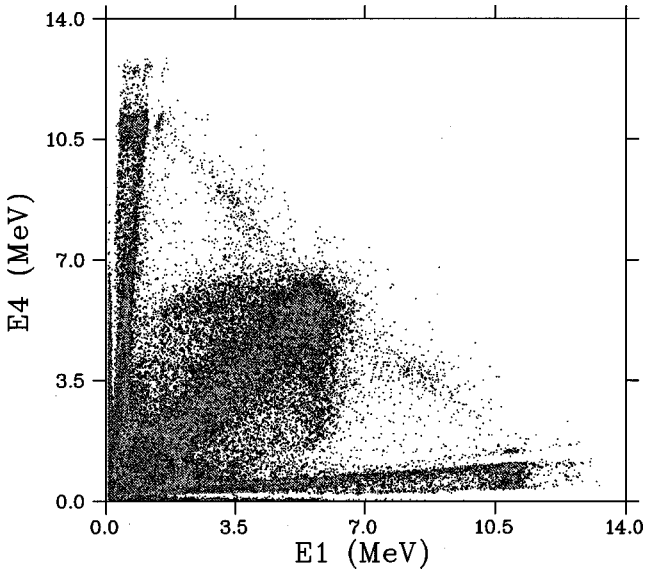

FIG. 5. Scatter diagram of double coincidences for telescopes S1 and S4 showing back-to-back spectra for this detector pair with 30 μm front detectors.

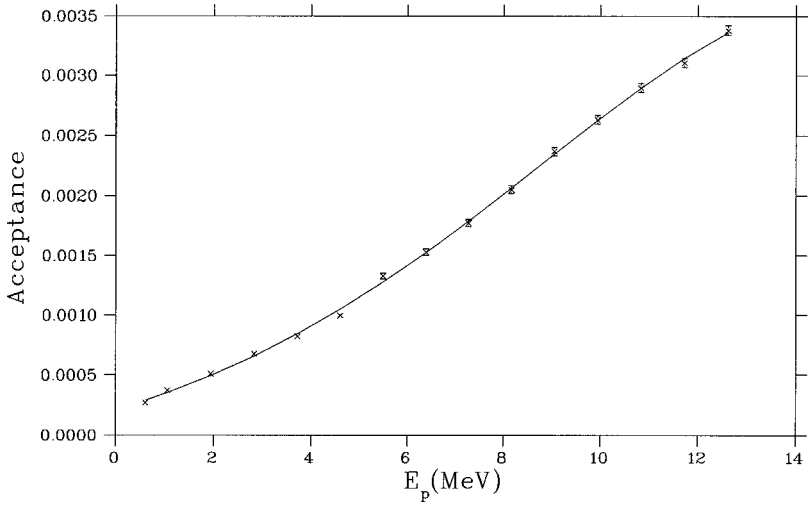

FIG. 6. Simulated kinematic efficiency of telescope S1 for detection of protons in coincidence with one or two α-particles in the ^{8}Be(g.s.)$+p$ channel as a function of proton energy. The crosses with the statistical error represent the calculated points. The smooth curve is a fourth order polynomial fit. Each point was simulated from 2×10^6 events.

IV. DATA ANALYSIS

A. Expt. 1: Decay through the ^{8}Be ground state

As noted in Sec. II B, the two sets of back-to-back coincident pairs S1-S4 and S2-S3 were used to select uniquely the decays of ^{9}B through the ground state of ^{8}Be. Events for this decay channel were simulated with the Monte Carlo program for a Gaussian source density and the geometry of Fig. 2. For the purposes of a demonstration, it was assumed that the excitation in ^{9}B consisted of broad levels at 2.8 and 12.2 MeV. The results of the S1-S4 simulation are shown in Fig. 4. In this figure, the coordinates of each point are the energies of the coincident pair of particles. The data for this channel [^{9}B breakup into ^{8}Be(g.s.)$+p$] are found exclusively in the nearly horizontal (slope$\approx$1/10) and nearly vertical (slope$\approx$10/1) bands.[6] This can be understood qualitatively by noting that, as the ground state of ^{8}Be is very narrow, only a very small energy ($Q_2=0.092$ MeV) is available for the breakup into two α particles, and the coincidences were obtained in back-to-back geometry. The protons are the higher-energy partners of the coincident pair. The sharp component of the bands corresponds to the detection of both α particles in the same detector. The experimental data for the S1-S4 pair are presented in a similar way in Fig. 5. Clearly an energy ratio cut incorporating the two bands will select those events associated with this channel. One can already see in this figure that ^{9}B states at about 2.8 and 12.2 MeV are strongly populated in the β decay of ^{9}C.

For each pair of back-to-back detectors two proton spectra can therefore be obtained by projection of the events selected by the ratio cuts onto their respective energy axes. It is evident from kinematics considerations that the coincidence efficiency for a given detector depends on the energy of the proton (i.e., the excitation energy in ^{9}B). Monte Carlo calculations were carried out to determine the coincidence efficiency as a function of proton energy for each of the counters. The efficiency curve for S1 is shown in Fig. 6. In order to explore the systematic errors associated with the efficiency curve, additional Monte Carlo calculations were

[6]The other events lying between the two bands are due mainly to decay of the 12.2 MeV state through the ^{5}Li ground state and the ^{8}Be first excited state and will be discussed in the next section.

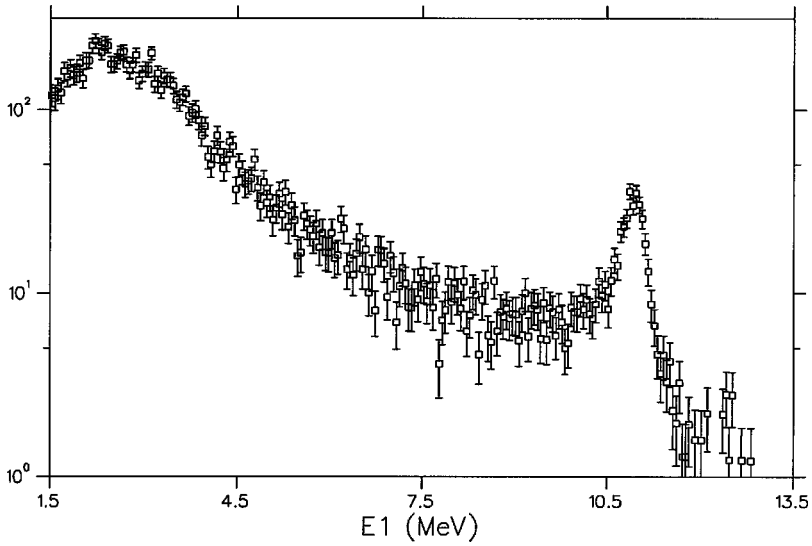

FIG. 7. Proton spectrum measured by Telescope S1 after applying a ratio cut to select the proton-α coincidences from the decay through the ^{8}Be(g.s.)$+p$ channel. A kinematic efficiency correction has been applied. The error bars include only statistical errors.

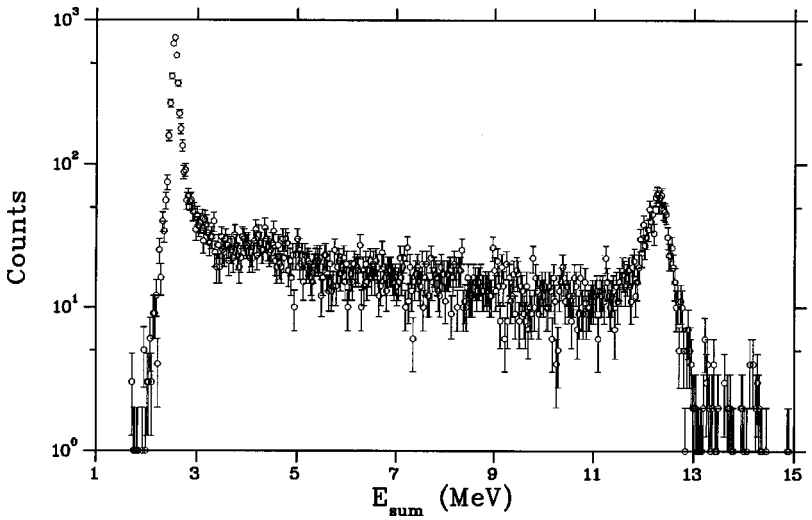

FIG. 8. Triple-coincidence energy-sum spectrum for SSDL, SSDR, and TL coincidences before efficiency correction.

carried out for assumed possible misalignments in the geometry and source position as well as the effects of hardware and software thresholds. The most serious effects on the branching ratios would be those resulting from changes in the energy dependence of the efficiency curve. Therefore, several efficiency curves, based on reasonable assumptions of uncertainties in source and threshold position, were produced by extensive Monte Carlo simulations. The extremes for the efficiency curves were then used in the analysis section to estimate the errors of the branching ratios. Energy straggling in the source for the low-energy particles would also constitute a small source of error; calculations indicate that such errors would be adequately included within the extremes described above.

The final proton spectrum for events associated with the detection of protons in S1, corrected for coincidence efficiency, is shown in Fig. 7. This spectrum along with those for proton detection in the other three detectors were used to calculate the relative β-decay branching ratios of ^{9}C to states which decay via the ground state of ^{8}Be (see Sec. V A 4).

B. Expt. 2: Decay through ^{5}Li ground state

1. Kinematics selection

The experimental two-dimensional coincidence energy plot is shown in Fig. 5 for the S1-S4 back-to-back geometry of expt. 1, while the Monte Carlo simulations for the decay of the 12.0 MeV state in ^{9}B through the ^{5}Li ground state and the ^{8}Be(3 MeV) state are shown in Fig. 4 for the S1-S4 back-to-back detector pair. This simulation shows a clustering of events on the diagonal ($E1=E4$) at approximately 6 MeV which corresponds to α-α coincidences (accompanied by two low-energy crescents). Two wings on nearly straight lines with negative slope emanating from the cluster at $E1=E4=6$ MeV are proton-α events from the decay through ^{5}Li. These events are, however, overlaid by those emanating from the 12 MeV$\rightarrow$ ^{8}Be(3 MeV) decay. This structure is clearly reproduced in the experimental results of Fig. 5. The approximate back-to-back geometry is kinematically favored for decays through the ^{5}Li channel because, in the subsequent breakup of the ^{5}Li recoil nucleus, the α particle receives only 1/5 of the breakup energy and has a very low velocity. Consequently, the vector addition of this velocity with the recoil velocity causes only a little deviation from back-to-back coincidences. Monte Carlo simulations were carried out for a set of excitation energies in ^{9}B from 2 to 14 MeV, for decays through both the ground state of ^{5}Li and the first excited state of ^{8}Be. The former produces a continuous set of mainly diagonal events at lower energies due to the decay of states of lower excitation energy in ^{9}B. The latter mode [^{8}Be(3 MeV)] also appears as events mainly on the diagonal but at a somewhat lower energy for the same excitation in ^{9}B. Clearly, for energies of about 4 MeV the back-to-back geometry cannot distinguish decays through the ground state of ^{5}Li from those through the first excited state of ^{8}Be.

To provide the required kinematic selectivity[7] at the lower energies, the geometry of expt. 2 was used. Triple coincidence events involving detectors SSDR, TL, and SSDL (Fig. 3) were selected for analysis, as detector TL was experimentally superior in resolution to detector TR. In this arrangement, detection of the coincident α particles in SSDR and TL provided the approximate back-to-back configuration, while detection of protons in SSDL provided the additional kinematic constraint necessary to distinguish between the two modes of decay. The large acceptance angles of the SSDs ensures adequate kinematic acceptance for the triple coincidences. The experimental triple coincidence spectrum is shown in Fig. 8. In the detailed kinematic analysis of these triple coincidences, a small number of events was identified where the proton was detected in either SSDR or TL. Since these events constituted less than 3.6% of the total, they were ignored. For the events of Fig. 5 the ratio of the number of events in the proton-α wings to that in the α cluster for the

[7]In principle, the precise determination of the vector momenta of two of the particles would completely define the kinematics of the sequential decay. This is not possible because of the finite size of the source and finite solid angles of the detectors.

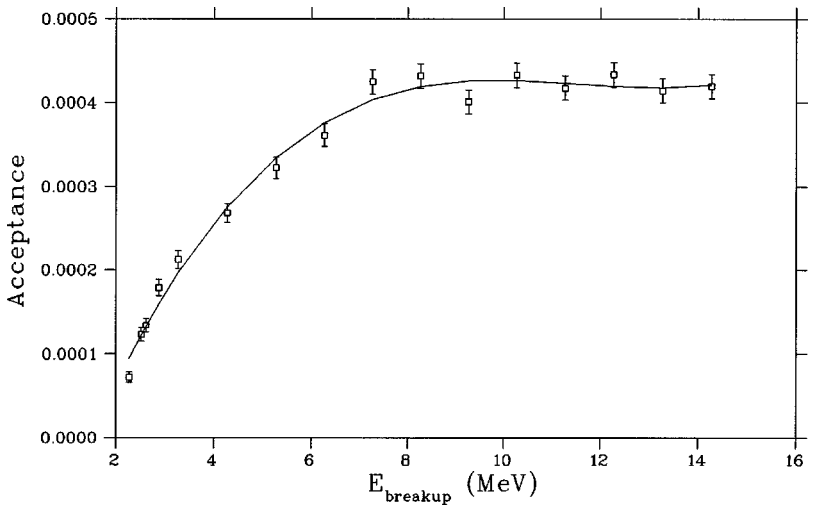

FIG. 9. Simulated triple-coincidence efficiency of SSDL, SSDR, and TL for the ^{9}B breakup through the ^{5}Li$(3/2^-)+\alpha$ channel as a function of the breakup energy. The squares with statistical errors represent the calculated points. The smooth curve is a fourth order polynomial fit. Each point was simulated from 2×10^6 events. In the region below 4.0 MeV, angular distributions for the $5/2^-$ ^{9}B state were used. For the rest of the points, an isotropic distribution was assumed corresponding to $J^\pi=3/2^-$.

decay of the 12.2 MeV state was compared with the Monte Carlo simulation. The experiment shows an excess of events in the proton-α wings relative to the simulations. This can be explained kinematically only by decays through higher excitations in ^{5}Li or ^{8}Be. A cut has been set on these events and the secondary breakup energy value Q_2 has been determined following Eq. (11). While there are certainly underlying events from the ^{5}Li decay of the $E_x=12.2$ MeV state, there is a clear peak at $Q_2=3$ MeV which can be identified with the first excited state of ^{8}Be. Therefore, this excess of counts is identified as a small branch from the $E_x=12.2$ MeV ^{9}B state through the first excited state of ^{8}Be.

2. Triple coincidence efficiencies and triple sum spectra

The Monte Carlo coincidence efficiency as a function of the excitation energy in ^{9}B was calculated for the SSDL, SSDR, and TL combination of detectors following the procedure outlined above. It was assumed that protons were detected in SSDL while α particles were detected in the other two detectors. As noted above, the angular correlation probabilities for each energy have to be included in the Monte Carlo calculation. Also threshold effects, as set experimentally or in the analysis, were simulated. This requires a knowledge of, or an *a priori* assumption about, the spins of the ^{9}B states and the relative contributions of these states at the energy in question in the experimental spectrum, to which the efficiency curve is to be applied (Fig. 8). The main contributors in this spectrum are the $J^\pi=5/2^-, E_x=2.34$ MeV, and $E_x=12.2$ MeV ^{9}B states, and the continuum between them. Consequently, in the region up to 4 MeV the angular correlation for $J^\pi=5/2^-$ with only the lowest allowed l value was assumed. Since the angular distribution for the 12.2 MeV state has been shown to be consistent with isotropy (see Sec. IVD), an isotropic correlation was taken for the entire region above 4 MeV. Low-energy cuts were incorporated for each detector which reflected those

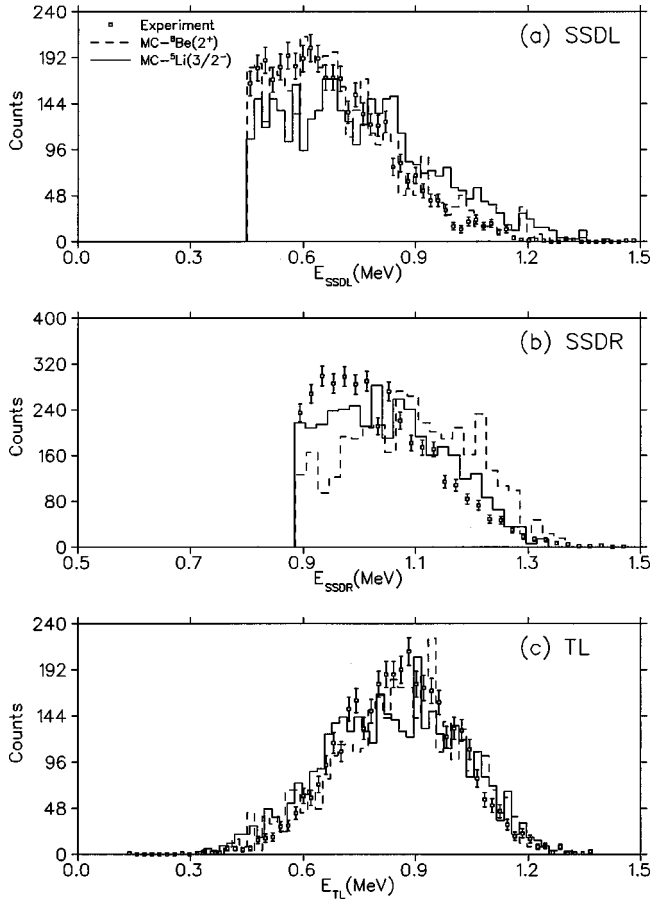

FIG. 10. A comparison between Monte Carlo (full line histograms) and experimental spectra of energies observed in the individual detectors from the breakup of the ^{9}B 2.34 MeV state via the ^{5}Li$(\frac{3}{2}^-)+\alpha$ channel after putting an energy threshold cut on SSDL and SSDR: (a) proton in SSDL, (b) α in SSDR, and (c) α in TL. For comparison, similar simulations for the breakup through the ^{8}Be(3 MeV) state are shown (dashed histogram) for an isotropic angular distribution.

imposed by the timing discriminators used for the experimental data. The efficiency curve is shown in Fig. 9.

The systematic errors of the efficiency curve were determined in a manner similar to that described in Sec. IV A. However, because of the uncertainties introduced by the angular correlation assumptions, the systematic errors here are greater than those for decay via ^{8}Be(g.s.). In addition, the application of an energy threshold for the timing cut has a more serious effect on the efficiency and is reflected in a suppression of the low-energy region of the efficiency curve. Timing cuts, as described in Sec. II C, were applied. With the efficiency corrections applied, these are the final data which will be used in Sec. V to determine the partial ^{9}C β-decay branching ratios to ^{9}B states that decay through the ground state of ^{5}Li.

In order to investigate the nature of decays at lower energies where overlap with possible decays through the first excited state of ^{8}Be can occur, a gate was set on events of Fig. 8 corresponding to the 2.34 MeV state of ^{9}B. The selected events for each detector are shown in Fig. 10 (points with error bars). The simulated Monte Carlo events for decays through both the ground state of ^{5}Li and the first excited state of ^{8}Be (isotropic distribution,[8] see Table I) are shown as separate histograms. Both distributions agree reasonably well, but not perfectly, with the data. Therefore a distinction between the ^{5}Li(g.s.) and ^{8}Be(3 MeV) decays is not possible in this energy region by kinematic constraints. Because in the continuum between 4 and the 12.2 MeV state no decay to the ^{8}Be(3 MeV) state is found, and because a high-energy tail of the 2.34 MeV peak is expected in this region, the ^{5}Li(g.s.) decay route is chosen here as the preferred scheme. In the subsequent text the transition will then be discussed as originating from a pure ^{5}Li(g.s.) transition even though a pure ^{8}Be(3 MeV) state transition has also been calculated and simulated. In Sec. V B, where a simulation of singles spectra from the derived branching ratios will be discussed, further arguments for a predominant ^{5}Li decay will be presented. However, in Ref. [15] it will be shown that there are problems related to the width of the 2.34 MeV state which make it likely that the decay is not really sequential. In this case both the ^{5}Li(g.s.) as well as the ^{8}Be(3 MeV) transitions are just extreme cases. The slight disagreement between data and MC simulations in Fig. 10 for both cases is attributed to the possible kinematics of a nonsequential decay.

A further corroboration of the MC calculations applied here is shown by the qualitative comparison shown in Fig. 11. The experimental data were selected from those of Fig. 8 with an energy gate set on the 12.2 MeV state of ^{9}B. The two-dimensional coincidence distributions for each pair of detectors are compared with those of the Monte Carlo simulations and show good qualitative agreement.

[8]For a $1-0.7P_2$ angular distribution of the $2.34\rightarrow{}^8$Be(3 MeV) transition, the histograms are very similar to those of an isotropic distribution.

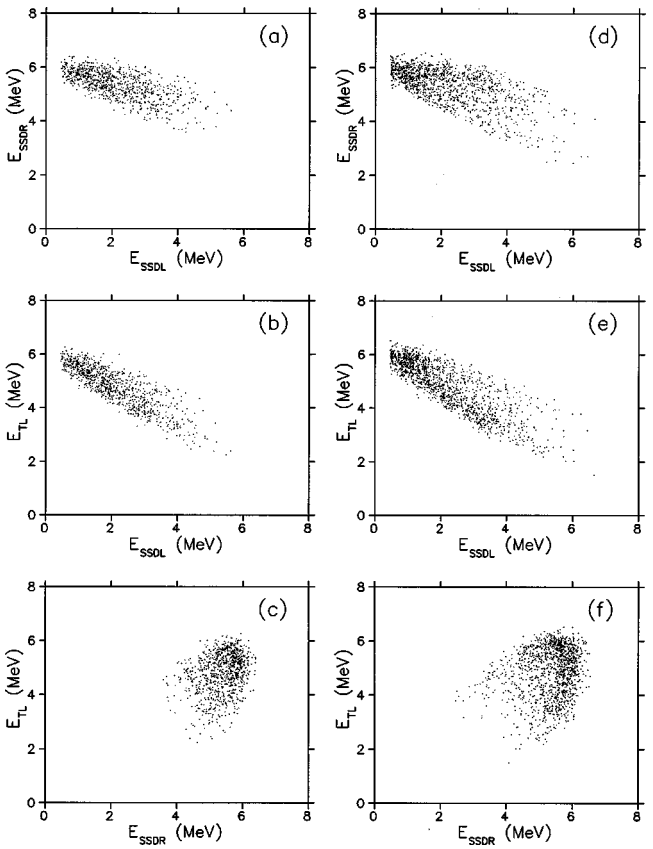

FIG. 11. Scatter diagram of energy-energy correlations for different detector combinations for the decay of the 12.2 MeV ^{9}B state: a comparison between the experimental (a)–(c) and Monte Carlo (d)–(f) data.

C. Decay of the ground state of ^{9}B

β decay to the ground state of ^{9}B can be identified by the detection of a low-energy proton emitted in the decay to the ground state of ^{8}Be ($Q=0.185$ MeV). Because of the very large β background, it is easiest to detect the low-energy protons with a thin detector gated in coincidence with a β particle in the plastic scintillator detector. The thin front detector of telescope TL in expt. 2 was used for this purpose. The β-gated particle spectrum is shown in Fig. 12. The low-energy proton peak at 0.164 MeV is prominent and the β background is negligible [the α particles from the breakup of ^{8}Be(g.s.) are too low in energy to be detected with this setup]. The events above the peak are all due to decays from higher excitations in ^{9}B. The energy threshold for the β detector was set at 4 MeV. The ratio between the area of the peak and the higher lying events (Fig. 12) is used in Sec. V A 4 to determine the β-decay branching ratio to the ground state of ^{9}B. However, this ratio is dependent upon the efficiency of detection of the β particle. A Monte Carlo program to simulate the response of the β detector was written using the CERN-developed program GEANT. It provides user-defined subroutines to track various particles through a user-specified geometry, simulating the physical processes that take place during the interaction, such as energy loss, multiple scattering, bremsstrahlung, pair production, and Compton scattering. Incorporated in the simulation were the

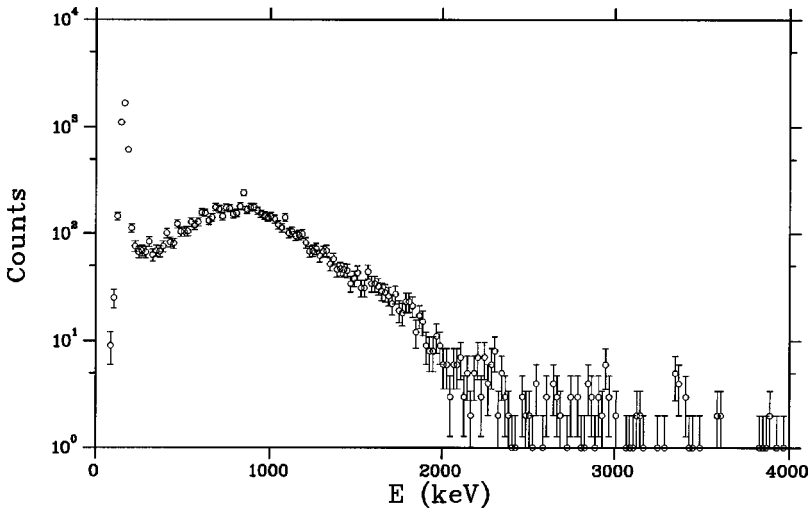

FIG. 12. Particle energy spectrum detected by the front detector of telescope TL (Fig. 3) in coincidence with a β particle in the plastic scintillator for $E_\beta > 4$ MeV (expt. 2).

experimental setup and the theoretical β-particle spectra. The desired output of the program, the energy deposited in the active volume of the detector, was recorded for each event (see Sec. V A 4).

D. Angular correlation—The spin of the 12 MeV state

The sum peak in the triple coincidence spectrum at approximately 12.4 MeV (Fig. 8) from the decay of the 12.2

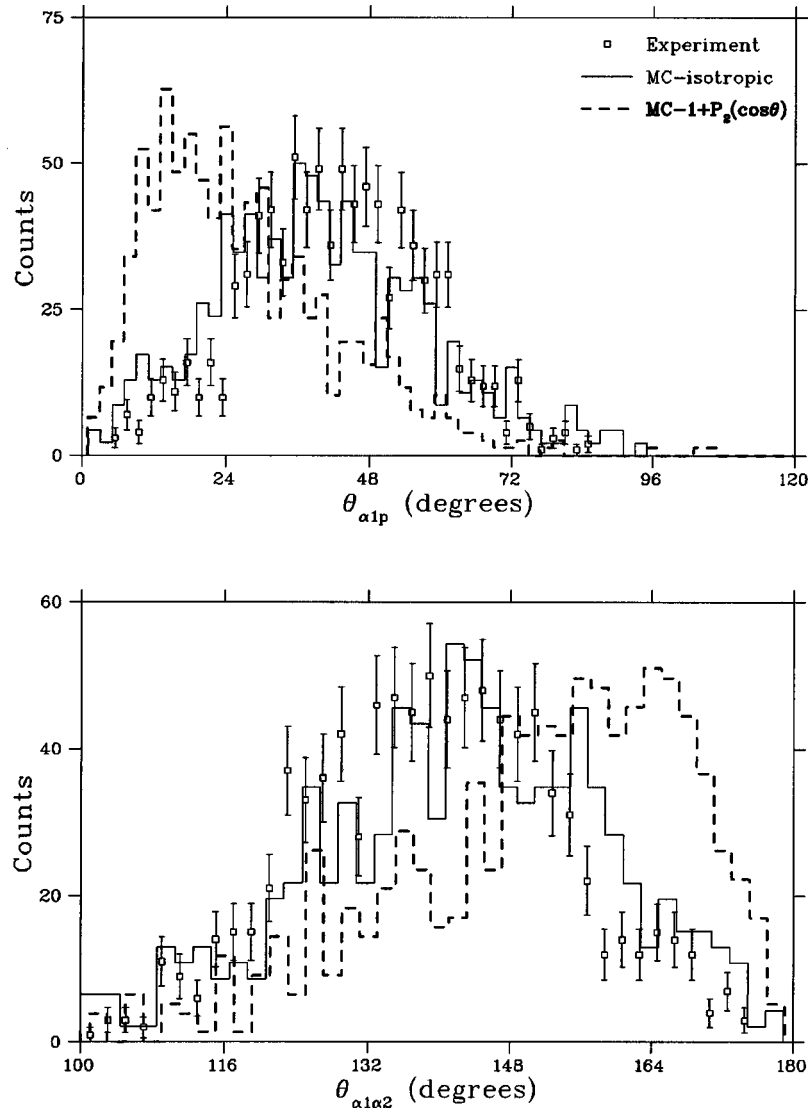

FIG. 13. Center-of-mass angular correlation between the first α particle and the particles from the secondary breakup in the decay of the 12.2 MeV ^{9}B state through the ^{5}Li$+\alpha$ channel. The solid line histogram is a Monte Carlo simulation that assumes a spin-parity of $J^\pi = 3/2^-$ for this state, with an isotropic angular distribution. The dashed line histogram is a simulation for a spin-parity of $J^\pi = 1/2^-$ for this state (Sec. III B). (a) shows the $\alpha 1$-p angular correlation and (b) the $\alpha 1$-$\alpha 2$ correlation.

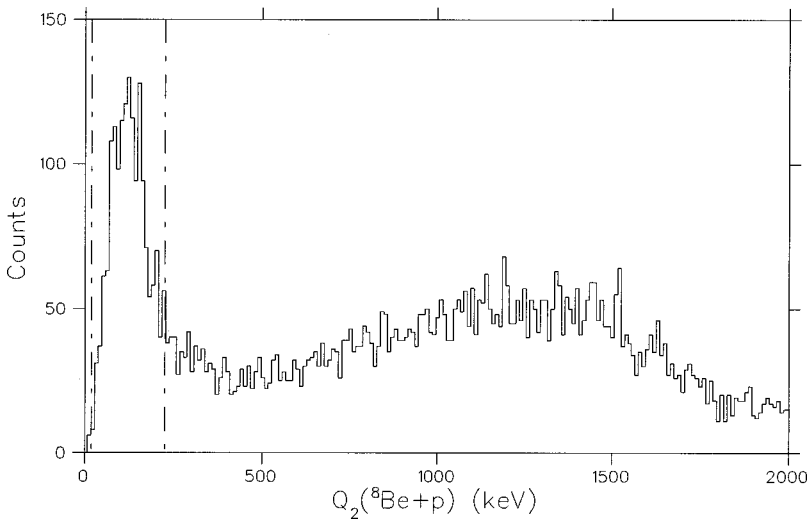

FIG. 14. Spectrum of the secondary breakup Q_2 value [Eq. (11)] made by SSDL-TR coincidences. The vertical dash-dotted lines mark the cut applied for ^{8}Be(g.s.) transitions on the breakup Q_2 spectrum of Fig. 15.

MeV state has been studied. The comparison of the Monte Carlo simulation with experiment has been noted above (see Fig. 11) and confirms these events to be mainly breakups through the ^{5}Li ground state. The center-of-mass angles between the first α particle and the secondary breakup particles were then determined for each event. A plot of these angular distributions and the comparisons made with the Monte Carlo simulations assuming a spin of either 3/2 or 1/2 is given in Fig. 13. From these plots, the spin of the 12.2 MeV state is determined to be 3/2 or greater. In Ref. [4] shell model results for the states in the ^{9}B nucleus are presented. In the high excitation region of ^{9}B ($E_x > 8$ MeV) only a $J^\pi = 3/2^-$ state is populated sufficiently by β decay to be identified with the 12.2 MeV state here. A nearby $J^\pi = 5/2^-$ state is not expected to show any significant decay via the ^{8}Be$+p$ ground state channel. Reference [4] therefore suggested a spin and parity $J^\pi = 3/2^-$ for this state, which is in agreement with our data.

E. Weak branches

β-decay branches to the most visible ^{9}B states, i.e., the ground state, and the $E_x = 2.34$, 2.8, 12.2, and 14.0 MeV states, can be found easily in the data. However, some weaker β-decay branches can also be identified.

To explore a breakup from the first-excited $1/2^+$ state of ^{9}B, the events in the low-energy region of the two-dimensional energy spectrum of expt. 2 were selected for study. These events were obtained using the SSDL-TR double coincidence detector combination. The values of Q_2 in Eq. (11) were calculated for these events and are plotted in the number distribution of Fig. 14. The events within the gate defined by the vertical dashed lines have the appropriate value of Q_2 for decay from the first excited state of ^{9}B. The proton energy spectrum, presented in Fig. 15, clearly shows events below 1.5 MeV. Careful fits to the ground state and higher-lying states ($J^\pi = 1/2^-, 5/2^-$) are necessary to determine the $J^\pi = 1/2^+$ fraction in this peak [15].

Fits to the triple sum spectrum (see Sec. V A 2) show an apparent excess of counts at $E_x = 2.7$ MeV suggesting a weak β-forbidden branch to the first $J^\pi = 5/2^+$ state in ^{9}B. The $E_x = 13.3$ MeV state is seen in the ^{8}Be$+p$ spectrum (Fig. 16) as a narrow peak with 2.8σ evidence; however, the evidence in the summed single spectrum is much clearer (see Sec. V B). At the known location of the isobaric analog state

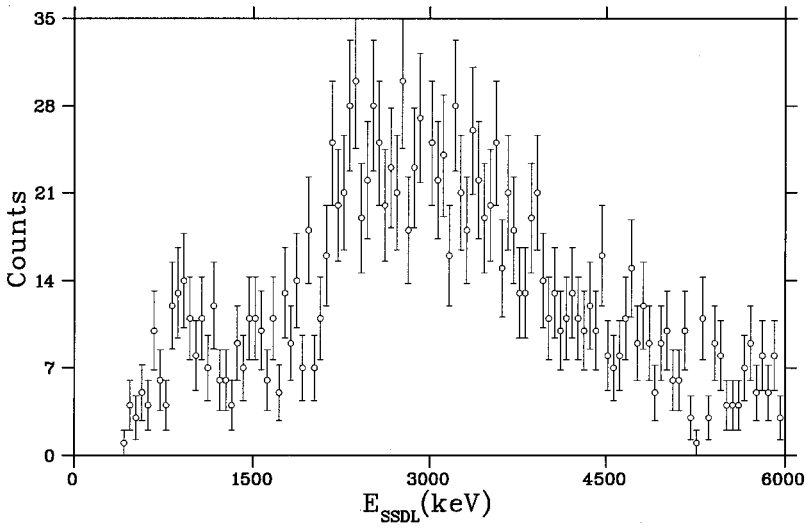

FIG. 15. Proton energy spectrum of SSDL-TR coincidences after the secondary decay energy cut applied on Q_2 (see Fig. 14). The broad peak near 3 MeV corresponds to the peak shown in Fig. 7 resulting largely from the 2.8 MeV state.

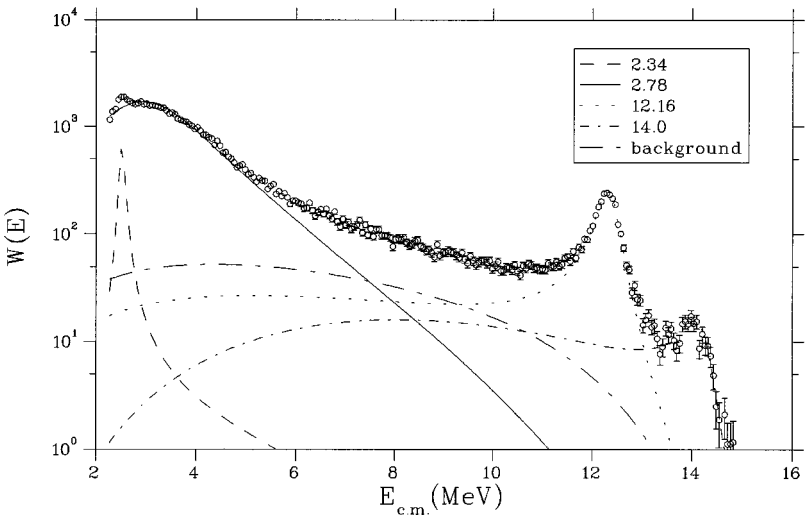

FIG. 16. Fit to the summed telescope spectrum (ratio cut) from expt. 1, corrected for efficiency. The fitted contribution from each ^{9}B state to the total spectrum is shown. The error bars on the data points represent statistical errors only. The component labeled background is a continuum arising from an assumed higher-energy state.

(IAS) in both spectra, a slight excess of counts is found in both spectra. The branching ratio found for the IAS branch ($\approx$0.006%) is consistent with a pure Fermi transition for which a branching ratio of 0.007% is expected.

V. RESULTS

A. Branching ratio determination

The steps involved in the phenomenological determination of the branching ratios will be discussed in this section. Here, the term ''phenomenological'' means that the branching ratios to apparent peaks are determined by using simplified fitting methods and Monte Carlo techniques (Sec. IV). While this formal description of states is largely consistent with previous work [5,4], it will be seen in a future publication [15] that fits using the *R* matrix allow a somewhat different interpretation of these apparent peaks and also permit an alternative description for that part of the spectrum that has been designated as the continuum. This interpretation indicates that part of the continuum does not show any obvious association with an apparent state. However, there are also some complications with the *R*-matrix method which will be discussed in Ref. [15].

In addition to the determination of branching ratios by the phenomenological method, the present analysis has also been found necessary for calibration of the absolute branching ratios of the two independent distributions [the ratio cut ^{8}Be(g.s.) and the triple sum spectrum] as well as of the ground state spectrum used in the later *R*-matrix fits [16]. The numerical effort required to calculate Monte Carlo distributions based on fitted *R*-matrix calculations is, in fact, prohibitive. Both the phenomenological and *R*-matrix methods give good fits to the data and reproduce the experimental spectra in Monte Carlo (back) simulations [16]. These are Monte Carlo simulations using the derived parameters to resimulate the experimental spectra (Sec. VB). The difference between the phenomenological and the full *R*-matrix methods is solely in the decomposition and therefore in the interpretation of (parts of) the data. In fact, it will be shown that branching ratios for broad interfering states are definition dependent [15] and therefore always require some interpretation.

Because many of the excited states of ^{9}B are broad, and because there is in all cases more than one decay channel available for the breakup, the procedure used in determining the decay branches involves analyzing the spectra for the different decay modes separately and relating the information obtained on the decay branches from one data set to another.

Each ^{9}B state populated in the β decay of ^{9}C is considered here to be an isolated resonance. The functions to be fitted are derived from those discussed in Sec. III A. In order to further minimize the computing time in the fitting, the relative shift functions for the ^{9}B states, $\Delta_{9\lambda}(E)$, were set to zero [Eq. (1)]. In addition, the total width of the ^{9}B state Γ_λ [see Eq. (2)] was assumed to be independent of energy (also see the later discussion in Ref. [15]). The fits used minimization of the least squares parameter χ^2 in the usual fashion.

The results for the fits to the ^{8}Be(g.s.)$+p$ spectrum are presented in Sec. V A 1. In Sec. V A 2, the results for the fits to the states decaying via the ^{5}Li($3/2^-$) channel are given. The procedure used in the normalization between the spectra for the two decay channels and the subsequent relative branch determination for the excited states of ^{9}B is discussed in Sec. V A 3. In Sec. V A 4, a determination of the relative strength of the ground-state transition to the strength of tran-

TABLE II. State energies, widths, and relative feeding factors obtained from the fit to the ^{8}Be(g.s.)$+p$ spectrum. The ^{9}B excitation energies (E_x) are obtained from $E_x = E_{\text{c.m.}} - 0.185$ MeV. In the last column the relative contribution of each state is given normalized to the intensity of the 2.8 MeV state.

E_x (MeV) in ^{9}B	Γ (MeV)	J^π	A_λ	Relative intensity
2.34	0.12	$5/2^-$	4.0	0.03$\pm$0.002
2.8	2.50	$1/2^-$	86.9	1
12.16	0.45	$3/2^-$	61.4	0.095$\pm$0.007
14.0	0.60		358.7	0.03$\pm$0.002
Background			181.6	0.09$\pm$0.01

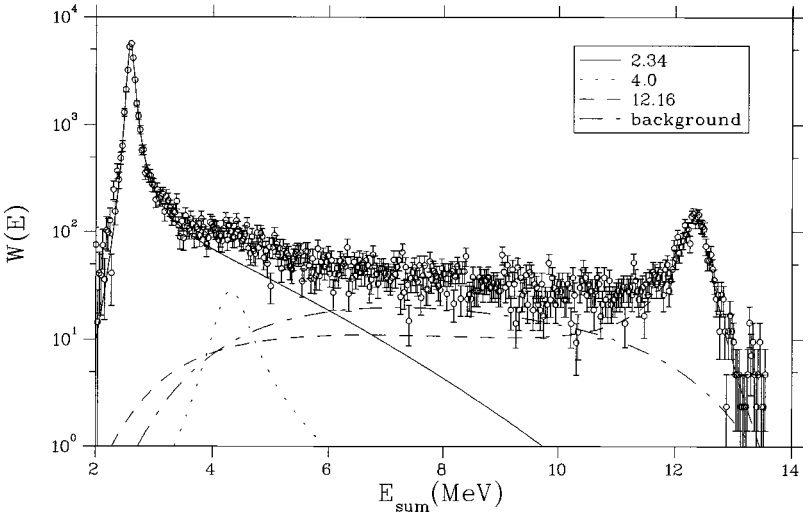

FIG. 17. Fit to the triple-coincidence energy-sum spectrum for SSDL, SSDR, and TL from expt. 2. The fitted contribution of each ^{9}B state to the total is shown. The error bars represent statistical errors only.

sitions to the excited states is discussed. This was done using the singles spectrum and the relative feeding factors obtained in Secs. V A 1, V A 2, and V A 3, respectively. This allows the final determination of the relative β-feeding factors as well as the determination of the breakup chain branches for the ^{9}B breakup (Sec. V B).

1. Relative branches for the decay through ^{8}Be(g.s.)+p channel (Expt. 1)

The proton spectrum from the breakup of ^{9}B $\rightarrow$ ^{8}Be(g.s.)+p has been discussed in Sec. IV A. After efficiency corrections the spectra from the four telescopes ($S1$ $\rightarrow S4$) were summed. This summed spectrum is shown in Fig. 16. The spectrum is composed mainly of a weak narrow peak near 2.5 MeV from the $5/2^-$ state, a broad peak around 3 MeV from the $1/2^-$ state, and peaks near 12.2 and 14.0 MeV. Included in the fit were these four states as well as a background state that is represented by a broad level at a higher excitation energy in ^{9}B.[9] The contribution from each level to the fit is shown in Fig. 16. The fitting parameters and the spin and parity assignments used in the fit are given in Table II. The intensity of each state normalized to the intensity of the 2.8 MeV state is given in the last column of this table.

2. Relative branches for the ^{5}Li+α channel (Expt. 2)

The triple coincidence spectrum measured by SSDL, SSDR and TL in expt. 2 has been discussed in Sec. IV B 2. This spectrum is treated as mainly resulting from breakups through the ^{5}Li+α channel (see Sec. IV B 2). A plot of the spectrum after efficiency corrections is given in Fig. 17. The x axis corresponds to the sum energy ($E_{\rm sum}=E_x$ $+0.277$ MeV) of the three particles detected in coincidence. The dominant features in this spectrum are the two peaks from the states at 2.34 and 12.2 MeV. There is also a bump near 4 MeV which is interpreted here as the breakup of the $E_x=2.8$ MeV, $J^\pi=1/2^-$ state; see also the discussion in Ref. [15]. These three peaks were included in the fitting routine. In addition, in order to account for the excess counts observed between the two peaks, a continuum (''background''), modeled by a wide state at higher excitation energy, was included in the fit. This background term is not correlated to the one used in modeling the ^{8}Be+p channel. The fitting parameters and the spin and parity assignments used in the fitting are given in Table III. The intensity of each state normalized to the intensity of the 2.34 MeV state is given in the last column of this table.

3. Normalizing the spectrum from the ^{5}Li+α channel to the ^{8}Be+p channel

Once the relative branches for both data sets are known, what remains in the determination of the relative β-feeding factors to the excited states of ^{9}B is to relate these relative branches by normalizing the ^{5}Li+α spectrum to the ^{8}Be $+p$ spectrum. The 2.34 and 2.8 MeV states, decaying almost entirely to ^{5}Li+α and ^{8}Be(g.s.)+p, respectively, were used

TABLE III. State energies, widths, and relative feeding factors obtained from the fit to the ^{5}Li+α spectrum. The ^{9}B excitation energies (E_x) are obtained from $E_x=E_{\rm sum}-0.277$ MeV. In the last column the relative contribution of each state is given normalized to the intensity of the 2.34 MeV state.

E_x (MeV) in ^{9}B	Γ (MeV)	J^π	A_λ	Relative intensity
2.34	0.10	$5/2^-$	17.4	1
(4.0) [a]	0.57	$(1/2^-)$[b]	0.24	0.020 ± 0.003
12.16	0.45	$3/2^-$	18.24	0.135 ± 0.007
Background	4.6	$(5/2^-)$[b]	80.7	0.106 ± 0.006

[a]Assumed to correspond to the lowest $J^\pi=1/2^-$ state at 2.8 MeV, see text.
[b]Assumed in fit.

[9]Because physically meaningful background terms would be interfering in one of the three allowed partial waves, no interpretation about the nature of this background is attempted; instead the reader is referred to Ref. [15].

TABLE IV. Relative ^{9}C β-decay branches to the excited states of ^{9}B obtained after normalizing the ^{8}Be(g.s.)$+p$ spectrum to the ^{5}Li$(3/2^-)+\alpha$ spectrum. The second column gives the relative intensity of each state with respect to the two separate spectra. The relative intensity (I_λ) with respect to the combined data is given in the third column. I_λ is normalized to the intensity of the ^{9}B(2.34) $\rightarrow$ ^{5}Li$(3/2^-)+\alpha$ transition.

E_x (MeV) in ^{9}B		
^{8}Be(g.s.)$+p$	$I_{^8\mathrm{Be}(0^+)+p}$	$I_\lambda = I_{^8\mathrm{Be}(0^+)+p}\left(\frac{N_{2.8\rightarrow{}^8\mathrm{Be}+p}}{N_{2.34\rightarrow{}^5\mathrm{Li}+\alpha}}\right)$
2.34	0.030	0.005 ± 0.0006
2.8	1.0	0.17 ± 0.018
12.16	0.095	0.016 ± 0.002
14.0	0.031	0.005 ± 0.0006
''Background''	0.088	0.015 ± 0.002
12.16$\rightarrow$ ^{8}Be$(2^+)+p$	[a]	0.034 ± 0.004
^{5}Li$(3/2^-)+\alpha$	$I_{^5\mathrm{Li}(3/2^-)+\alpha}$	$I_\lambda = I_{^5\mathrm{Li}(3/2^-)+\alpha}$
2.34	1.0	1.0 ± 0.19
(4.0)	0.020	0.019 ± 0.004
12.16	0.135	0.135 ± 0.014
''Background''	0.11	$0.106^{+0.05}_{-0.04}$

[a]Measured from the singles proton spectrum.

for the normalization. The ratio of the decay branches of these two states was determined from the two-dimensional (SSDR-TL) coincidence spectrum [16]. After making corrections for the acceptances for these two channels, the ratio of the strengths of the two branches was found to be $N_{2.34\rightarrow{}^5\mathrm{Li}+\alpha}/N_{2.8\rightarrow{}^8\mathrm{Be}+p}=5.8\pm0.6$. Using this ratio, the ^{8}Be$+p$ spectrum was normalized to the ^{5}Li$+\alpha$ spectrum. In the fourth column of Table IV, the relative intensities of each level in the total spectrum (I_λ), calculated from the normalization factor and the relative yields determined in Secs. V A 2 and V A 3, are listed. Consistent results for this branching ratio were also obtained relating the different decay channels of the 12.2 MeV state to one another.

4. Determination of the ground-state branching ratio from the β-particle spectrum

The analysis of the β-particle coincidence spectrum and the decay of ^{9}C through the ground state of ^{9}B have been discussed in Sec. IV C. This spectrum (Fig. 12) was used to determine the ratio of the β-feeding factor of the ground state to the sum of the feeding factors of all the excited states of ^{9}B. This was done by simulating the β-particle coincidence spectrum resulting from the breakup of all states of ^{9}B and comparing the experimental spectrum with that generated by the Monte Carlo simulation.

In order to simulate the contribution of each level to the particle spectrum recorded in coincidence with β particles in the β detector, it was necessary to include the distortion of the spectral shape of the ^{9}B states caused by the coincidence requirement. Due to the low-energy cutoff of the β detector (4 MeV), the particle-β coincidence efficiency is dependent on the ^{9}B energy into which the transition takes place. This energy-dependent efficiency was calculated for β spectra for a number of excitation energies in ^{9}B by Monte Carlo simulation (Secs. III C, IV C). The efficiency is then the ratio of the number of detected events that are above a certain β energy (in this case 4 MeV) to the total number of the detected events, i.e., $\varepsilon(E)=N_{(E_\beta>4\ \mathrm{MeV})}/N_{\mathrm{total}}$. The calculated efficiency curve $\varepsilon(E)$ is shown in Fig. 18. The spectral shape observed in the particle-β-coincidence spectrum $W'_\lambda(E)$ is then given by

$$W'_\lambda(E)=W_\lambda(E)\varepsilon(E), \tag{12}$$

where $W_\lambda(E)$ is the spectral shape for a ^{9}B state λ. The mean value of the efficiency, $\langle\varepsilon_\lambda(E)\rangle$, for each ^{9}B state used in the simulation is determined from

$$\langle\varepsilon_\lambda(E)\rangle=\frac{\int_0^{Q_\beta}\varepsilon(E)W_\lambda(E)dE}{\int_0^{Q_\beta}W_\lambda(E)dE}. \tag{13}$$

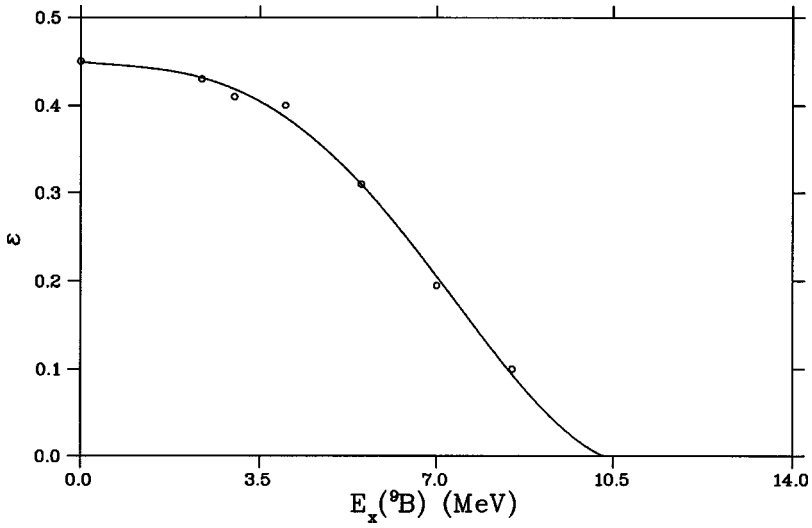

FIG. 18. Monte Carlo-simulated efficiency $\varepsilon(E)$ for detection of β particles with $E_\beta>4$ MeV in the scintillation detector used in expt. 2, as a function of ^{9}B excitation energy.

TABLE V. Relative contributions of the ^{9}B states decaying to the ^{5}Li$(3/2^-)+\alpha$ channel in the particle-β coincidence spectrum. The number of simulated events N (column 5) is equal to the results from the fit: I'_λ (column 4).

E_x (MeV) in ^{9}B	I_λ	$\langle\varepsilon_\lambda(E)\rangle=\frac{\int\varepsilon(E)w_\lambda(E)dE}{\int w_\lambda(E)dE}$	$I'_\lambda=I_\lambda\langle\varepsilon_\lambda(E)\rangle$	N
2.34	1.0	0.421	0.421	2.5×10^6
(4.0)	1.96×10^{-2}	0.373	7.15×10^{-3}	42,450
12.16	0.135	0.095	1.29×10^{-2}	76,300
Background	0.106	0.178	1.90×10^{-2}	112,225

The relative strength of each state in the particle-β spectrum I'_λ is therefore given by

$$I'_\lambda=I_\lambda\langle\varepsilon_\lambda(E)\rangle, \tag{14}$$

where I_λ is the relative strength of the ^{9}B state determined in Sec. V A 3, i.e.,

$$I_\lambda=\int_0^\infty W_\lambda(E)dE. \tag{15}$$

The spectral shapes $W'_\lambda(E)$ and the relative intensities I'_λ were used in simulating the particle-β spectrum.

In the fourth columns of Tables V and VI, the relative contributions of each state to the β-particle spectrum are calculated from the relative branches (column 2) and the β-detector efficiency (column 3). The number of simulated events is listed in the last column. 2.5×10^6 events were simulated for the ^{9}B$(2.34)\rightarrow{}^5$Li$+\alpha$ decay. The number of events for the remaining states was determined accordingly. The ground state branch, the only unknown variable in the simulation, was first arbitrarily assigned to have the same branch as the second excited state. The relation between the ground state branching ratio B(g.s.) and the branching ratio to the 2.34 MeV state $B(2.34)$ was determined by calculating the ratio of the counts under the ground state peak to the counts for the rest of the spectrum in both the experimental ($R_{\rm exp}$) and the Monte Carlo ($R_{\rm mc}$) data and by comparing these ratios (Figs. 12 and 19). The branching ratios for these two states are then found to be related by the expression

$$B(\text{g.s.})=\left(\frac{R_{\rm mc}}{R_{\rm exp}}\right)B(2.34)=(1.33\pm0.13)B(2.34). \tag{16}$$

B. Final branching ratios and reconstruction of the singles spectra

Using relation (16), the absolute branching ratio values were calculated and are given in Table VII. The energies of the states were taken from the fits to the ^{8}Be(g.s.)$+p$ spectrum where a good energy calibration was available. Because most states extend over a large energy range, the value of $B_{\rm GT}$ (except for the ground state transition) was calculated using an averaged inverse Fermi function folded over the distribution of each individual state and is given by

$$\langle B_{GT}\rangle=\frac{K}{t_{1/2}}\frac{\int_0^{Q_\beta}[1/f(E)]W(E)dE}{\int_0^{Q_\beta}W(E)dE}, \tag{17}$$

with $K=6177$ s and $t_{1/2}$ the partial half-life for the decay to that state. The logft value is then given by [4]

$$ft=\frac{K}{\langle B_{GT}\rangle}, \tag{18}$$

and is listed in Table VII.[10] Clearly the state at 12.2 MeV shows a very large Gamow-Teller strength making it a significant part of the Gamow-Teller giant resonance as found from the GT (Ikeda) sum rule. Errors were derived as discussed in Sec. IV by Monte Carlo–simulated variations of the efficiency curves, beam spot positions and other significant parameters. The errors are systematic; statistical errors are comparatively small. While the errors are highly correlated (because of the 100% sum rule for all branches and the different normalizations applied here), they are treated as independent of one another, i.e., likely somewhat larger than necessary. Energies of states are taken from the fits. Widths are defined in Eq. (2) and are therefore formal.

Using these branching ratios, the single event spectrum of the telescopes was simulated and compared with the experimental singles spectrum to check for consistency. For the low-energy part, the experimental spectrum used for comparison is the β-particle coincidence spectrum measured by TL owing to the background due to β particles in the measured singles spectrum. Figure 20 shows the low-energy part (below 4 MeV) of this spectrum. The spectrum obtained by Monte Carlo simulation has been normalized to the experimental spectrum by matching the counts under the proton peak at 164 keV. For the decay of the 2.34 MeV state a pure transition through ^{5}Li(g.s.) was assumed. If a transition

[10]Reference [5] uses $ft=[6141s/(G_A^2/G_V^2)B_{\rm GT}]$ for Gamow-Teller transitions with an unquenched $G_A^2/G_V^2=1.59$. G_A and G_V are the axial vector and vector coupling constants in β decay, respectively. Following Ref. [4] a quenched value for $G_A^2/G_V^2\approx1$ is taken here. When values of $B_{\rm GT}$ are compared with Ref. [5], the values here have to be divided by 1.58. Reference [5] uses a similar averaging procedure for $B_{\rm GT}$ to that described here.

TABLE VI. Relative contributions of the ^{9}B states decaying to the ^{8}Be(g.s.)$+p$ channel in the particle-β coincidence spectrum. The ground state branch has been arbitrarily assigned the same branching ratio as the 2.34 MeV state of ^{9}B. The number of simulated events N (column 5) is equal to the results from the fit: I'_λ (column 4).

E_x (MeV) in ^{9}B	I_λ	$\langle\varepsilon_\lambda(E)\rangle=\frac{\int\varepsilon(E)w_\lambda(E)dE}{\int w_\lambda(E)dE}$	$I'_\lambda=I_\lambda\langle\varepsilon_\lambda(E)\rangle$	N
0.0	1	0.450	0.450	2.67×10^6
2.34	5.08×10^{-3}	0.426	2.16×10^{-3}	12 852
2.8	0.17	0.405	6.96×10^{-2}	413 250
12.16	1.6×10^{-2}	0.137	2.24×10^{-3}	13 300
14.0	5.2×10^{-3}	0.134	7.04×10^{-4}	4180
Background	1.5×10^{-2}	0.287	4.35×10^{-3}	25 800
12.16[^{8}Be$(2^+)+p$]	3.4×10^{-2}	0.095	3.23×10^{-3}	19 000

through the ^{8}Be(3 MeV) state is chosen, no good match to the spectrum can be obtained [16]. In particular, the peak at about 0.9 MeV in Fig. 20 is then shifted in the simulations to higher energies. It is also obvious that, regardless of the decay sequence, the data presented in Fig. 20 do not allow a significant change in the branching ratio of the 2.34 MeV state corresponding to the peak at 0.9 MeV. For the high-energy part (above 4 MeV), the singles spectrum measured by telescope 2 in expt. 1 was used. This spectrum is given in Fig. 21. The proton peak for the 12.2 MeV state was used in the normalization. Clearly, in both spectra, the qualitative features of the singles spectra are well reproduced by the Monte Carlo simulation. Minor inconsistencies are attributed to (i) a not entirely correct state shape using the approximations described above and (ii) incomplete knowledge of angular momentum fractions, in particular, in the continuum region.

VI. CONCLUSION

In this first of two papers about the ^{9}C study at TISOL, there has been a description of how the experiment was performed and how the data were analyzed. The properties of visible states have been discussed and it has been demonstrated that coincidence techniques can indeed deliver results with respect to different breakup modes and angular momenta. The price to be paid for this additional information is that extensive Monte Carlo calculations are necessary to compare with the experimental results. Only with these simulations can a consistent interpretation of the data be achieved.

While a complete, fully consistent treatment of the data using both *R*-matrix theory and Monte Carlo methods would be desirable, such an undertaking is well beyond present day computing speeds. Therefore, the approach employed here was to fit the visible states by a modified Breit-Wigner form (Sec. III A), taking the energy dependence of the secondary compound states ^{5}Li and ^{8}Be into account, to allow a first iteration in deriving the branching ratios of the apparent states. As a final result, the branching ratios to and the decays from these states are listed in Table VII together with additional information from the present work and the literature. In a second article [15], it will be shown how these apparent states can be reinterpreted by applying *R*-matrix theory. In particular, a new interpretation of the ''background'' contributions to the ^{9}B decay will be derived, suggesting that the ''background'' to a large fraction is resulting from the coherent and incoherent sum of the ^{9}B ground state and unidentified states above the β threshold.

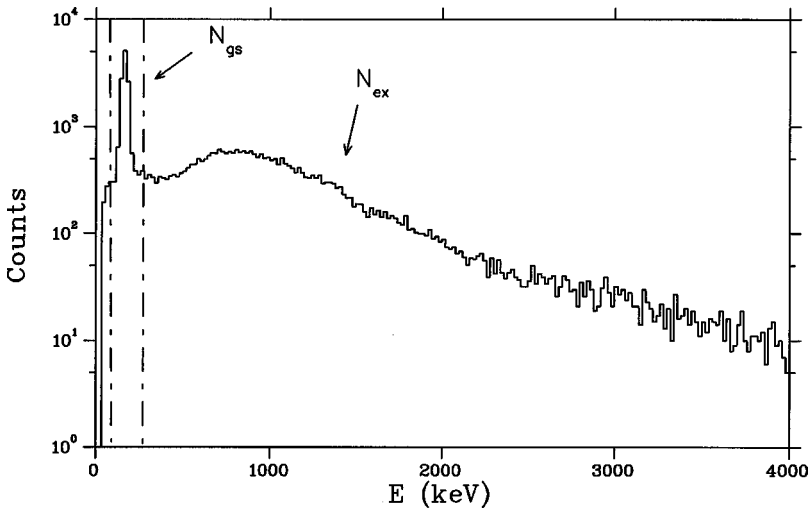

FIG. 19. Simulated particle energy spectrum in detector TL in coincidence with a β particle ($E_\beta>4$ MeV) detected by the plastic scintillator. This spectrum was compared with the experimental spectrum (Fig. 12) in calculating the ground-state branching ratio in the ^{9}C β decay.

TABLE VII. Level energies and branching ratios to states populated in the β-delayed particle decay of ^{9}C. B_p and B_α denote branching ratios to ^{8}Be (ground state and $E_x=3$ MeV state) and the ^{5}Li ground state relative to the total number of β decays. ''Background'' labels the fraction of the branching ratio which is due to states above $E_x=15$ MeV or states too broad to allow a unique identification to be made. B_{GT} is calculated using Eq. (17) and logft employing Eq. (18).

E_x (MeV)	J^π	B_β [%]	B_p [%]	B_α [%]	log ft	$\langle B_{GT}\rangle$
0.0	$\frac{3}{2}^-$	46.9±5.0	46.9±5.0 [a]	[b]	5.38	0.026±0.003
2.34±0.03	$\frac{5}{2}^-$	35.2±6.7	0.18±0.02 [a]	35.0±6.7 [c]	5.01	0.061±0.013
2.8±0.2	$\frac{1}{2}^-$	6.7±0.7	6.0±0.6	0.7±0.1 [d]	5.61	0.015±0.002
12.16±0.10	$\frac{3}{2}^-$ [e, f]	6.8±0.7	1.8±0.2 [g]	5.0±0.5	3.39	2.50±0.25
13.3±0.1		0.0020±0.0004	0.0020±0.0004	[b]	5.79	0.010±0.003
14.0±0.2	[h]	0.19±0.02	0.19±0.02	[b]	4.17	0.42±0.05
Background [i]		$4.2^{+2.1}_{-0.7}$ [j]	0.5±0.1	$3.7^{+2.0}_{-0.6}$ [j]	4.17	$0.42^{+0.21}_{-0.07}$ [i]

[a] ^{8}Be(g.s.) only.
[b] No evidence found for α breakup; assumed small.
[c] ^{5}Li(g.s.) and ^{8}Be(3 MeV) state decay not necessarily distinguishable. Arguments for a preferred ^{5}Li(g.s.) transition are presented in the text.
[d] Breakup through both ^{5}Li and ^{8}Be(3 MeV) are possible.
[e] $J^\pi > 1/2^-$, see text.
[f] Suggested from fit [15].
[g] 0.58±0.07% for ^{8}Be(g.s.) and 1.2±0.2% for ^{8}Be(3 MeV).
[h] See discussion in Ref. [15].
[i] From states which cannot be identified uniquely, see text.
[j] Error large and asymmetric due to unknown spin composition.

All of the states of ^{9}B that have been seen previously in β-decay measurements have been clearly observed in the present work. In addition, a strongly populated state at $E_x=14.0$ MeV and a weakly populated, narrow state at 13.3 MeV were found. There is an indication of a β decay to the first-excited ($1/2^+$) state of ^{9}B, for which the apparent state energy (without having performed detailed fits) appears to be near the lower values quoted in the theoretical literature [13]. For the first time in the breakup studies of ^{9}B, breakup channels of many of the ^{9}B states are clearly identified. It was found that the ^{9}B ground state (for phase space reasons), the $E_x=2.8$ MeV ($J^\pi=1/2^-$) state, and the $E_x=14$ MeV state decay preferably to the ^{8}Be(g.s.), but the continuum and the 12.16 state have a preference for ^{5}Li+α breakup which makes this mode dominant in the high-energy excitation region of ^{9}B. Thus it would be desirable to repeat the cluster model calculations of Ref. [25] in which it was assumed that all levels broke up into ^{8}Be(g.s.)+p. The 2.34 MeV state, corresponding to the second largest ^{9}C decay branch, has only a small branch to the ^{8}Be(g.s.). The relative decay branch to the ^{5}Li(g.s.) and the ^{8}Be(3 MeV) state remains unresolved, though arguments for a preference of the ^{5}Li(g.s.) channel are given. It will be suggested in Ref. [15] that this decay is not necessarily sequential.

Furthermore most of the Gamow-Teller strength of the ^{9}C decay is found leading to an excitation energy of above 10 MeV in ^{9}B and, indeed, a fair fraction of the total Gamow-Teller strength of ^{9}B is observed in this experiment accord-

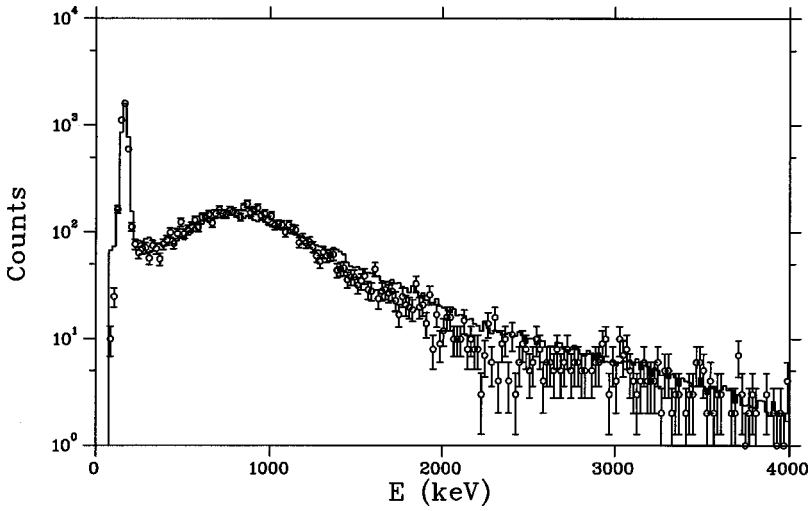

FIG. 20. A comparison of the singles ''reconstructed'' spectrum with the experimental data (telescope TL) in the low-energy region. The experimental data are shown by the open circles, and the Monte Carlo simulations by the histogram.

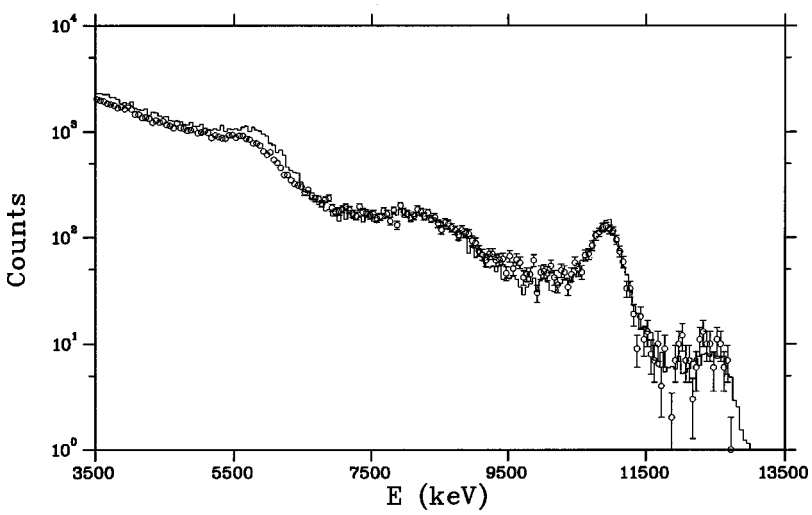

FIG. 21. A comparison of the singles ''reconstructed'' spectrum with the experimental data in the high-energy region. The experimental data are shown by the open circles, and the Monte Carlo simulations by the histogram.

ing to the Ikeda sum rule. Following the discussion in Ref. [4] the 12.2 MeV state can be regarded as the antianalog $T=1/2$ state to the $T=3/2$ analog state at 14.7 MeV. The arguments in Ref. [4] are based both on the GT strength of this state as well as on the energetic spacing between the 12.2 and 14.7 MeV IAS states.

Relatively poor agreement was found in the present work between the branching ratios of ^{9}B states with low excitation energy and those given in Ref. [4]. This can be attributed to (i) a different description of the shapes of states in this work relative to Ref. [5] and (ii) some of the corrections and cuts applied in Ref. [4]. By applying some significant changes on both points to the present data, the poor agreement can be lessened but not completely resolved. Good agreement is found with the range of Gamow-Teller squared matrix elements B_{GT} suggested in the shell model calculations of Ref. [4] for all states identified there. The strength of the 14 MeV ^{9}B state corresponds well with that of the next higher $J^\pi=1/2^-$ state above the $3/2^-$ state in the shell model calculations of Ref. [4]. For the shell model calculations of Ref. [26] excellent agreement is found for the logft values of the ground state and the 12.2 MeV state and, if identified as $1/2^-$, for the 14.0 MeV state. Poorer agreement is found for the 2.34 and 2.8 MeV states.

In Table VII, good agreement of the branching ratios with those of Ref. [5] is found, if the 2.8 MeV state of the present work is added to what has been referred to as background or continuum here. The latter contribution to the decay is found in the present work not to be part of the 2.8 MeV, $J^\pi=1/2^-$ state. It is also necessary to assume only one mirror state at 11 MeV in ^{9}Be instead of the two reported in the decay of ^{9}Li for the 12.2 MeV state in ^{9}B. While there is only one apparent state in the ^{9}B data at 12 MeV, some R-matrix fits (though inconsistent with the shell model state structure) suggest [15] that this state may be degenerate with a contribution from a close $J^\pi=1/2^-$ state. If this interpretation is adopted, there are no longer the major differences between the logft values of ^{9}C and ^{9}Li claimed in Refs. [4,5]. The Gamow-Teller matrix elements B_{GT} are too sensitive to the state shape functions to allow a definitive comparison, unless ^{9}Li decay data of the same quality as the present ^{9}C data become available, and are analyzed with the same method. In a future publication [15], it will be shown how the spectra we have found can be reinterpreted using definitions of branching ratios inherent to R-matrix theory [21].

ACKNOWLEDGMENTS

The help of TRIUMF operations and staff, in particular H. Sprenger, H. Biegenzein, and P. Machule, in making this experiment possible is gratefully acknowledged. Comments of Professor R. Sherr from Princeton University on an early version of this manuscript are highly appreciated. We are particularly grateful for comments on the manuscript made by Professor F. Barker of the Australian National University. Financial support from the Natural Sciences and Engineering Research Council of Canada for some of the collaborators and the National Research Council of Canada for others is gratefully acknowledged.

[1] J.C. Hardy, R.I. Verrall, R. Barton, and R.E. Bell, Phys. Rev. Lett. **14**, 376 (1965).
[2] J.E. Esterl, D. Allred, J.C. Hardy, R.G. Sextro, and J. Cerny, Phys. Rev. C **6**, 373 (1972).
[3] F. Ajzenberg-Selove, Nucl. Phys. **A490**, 1 (1989).
[4] D. Mikolas, B.A. Brown, W. Benenson, L.H. Harwood, E. Kashy, J.A. Nolen, Jr., B. Sherrill, J. Stevenson, J.S. Winfield, Z.Q. Xie, and R. Sherr, Phys. Rev. C **37**, 766 (1988).
[5] G. Nyman, R.E. Azuma, P.G. Hansen, B. Johnson, P.O. Larsson, S. Mattson, A. Richter, K. Riisager, O. Tengblad, K. Wilhelmsen, and the ISOLDE Collaboration, Nucl. Phys. **A510**, 189 (1990).
[6] A.C. Fonseca, J. Revai, and A.V. Matveenko, Nucl. Phys. **A326**, 182 (1979).
[7] J. Revai and A.V. Matveenko, Nucl. Phys. **A339**, 448 (1980).
[8] W. von Oertzen, Z. Phys. A **354**, 37 (1996).
[9] N. Arena, S. Cavallaro, G. Fazio, G. Giardina, A. Italiano, and F. Mezzanares, Phys. Rev. Lett. **57**, 1839 (1986).

[10] M. Burlein, H.T. Fortune, P.H. Kutt, R. Gilman, R. Sherr, and J.D. Brown, Phys. Rev. C **38**, 2078 (1988).
[11] W.N. Catford, L.K. Fifield, E.L. Reber, K.W. Kemper, and J.D. Brown, Nucl. Phys. **A550**, 517 (1992).
[12] M.A. Tiede, K.W. Kemper, N.R. Fletcher, D. Robson, D.D. Caussyn, S.J. Bennet, J.D. Brown, W.N. Catford, C.D. Jones, D.L. Watson, and W.D.M. Rae, Phys. Rev. C **52**, 1315 (1995).
[13] F.C. Barker, Phys. Rev. C **53**, 2539 (1996).
[14] S.E. Woosley and R.D. Hoffman, Astrophys. J. **395**, 202 (1992).
[15] L. Buchmann *et al.* (unpublished).
[16] E. Gete, Ph.D. thesis, University of British Columbia, 2000.
[17] L. Buchmann, J. Vincent, H. Sprenger, M. Dombsky, J.M. D'Auria, P. McNeely, and G. Roy, Nucl. Instrum. Methods Phys. Res. B **62**, 521 (1992).
[18] M. Dombsky, L. Buchmann, J.M. D'Auria, P. McNeely, G. Roy, H. Sprenger, and J. Vincent, Nucl. Instrum. Methods Phys. Res. B **70**, 125 (1992).
[19] M.J.G. Borge, H. Cronberg, M. Cronqvist, H. Gabelmann, P.G. Hansen, L. Johannsen, B. Johnson, S. Mattson, G. Nyman, A. Richter, K. Riisager, O. Tengblad, and M. Tomaselli, Nucl. Phys. **A490**, 287 (1988).
[20] R.E. Azuma, L. Buchmann, F.C. Barker, C.A. Barnes, J.M. D'Auria, M. Dombsky, U. Giesen, K.P. Jackson, J.D. King, R.G. Korteling, P. McNeely, J. Powell, G. Roy, J. Vincent, T.R. Wang, S.S.M. Wong, and P.R. Wrean, Phys. Rev. C **50**, 1194 (1994).
[21] F.C. Barker and E.K. Warburton, Nucl. Phys. **A487**, 269 (1988).
[22] A.M. Lane and R.G. Thomas, Rev. Mod. Phys. **30**, 257 (1958).
[23] F. C. Barker (private communication).
[24] S. Devons and L. J. B. Goldfarb, *Encyclopedia of Physics, Vol. 42, Nuclear Reactions 3*, edited by S. Fluegge (Springer, Berlin, 1957), p. 362.
[25] P. Descouvement, Phys. Rev. C **39**, 1557 (1989).
[26] F.C. Barker, Nucl. Phys. **83**, 418 (1966).